Development 140, 639-648 (2013) doi:10.1242/dev.086702

Sox17 haploinsufficiency results in perinatal biliary atresia and hepatitis in C57BL/6 background mice

Mami Uemura[1,2,*], Aisa Ozawa[1,*], Takumi Nagata[1], Kaoruko Kurasawa[1], Naoki Tsunekawa[1], Ikuo Nobuhisa[3], Tetsuya Taga[3], Kenshiro Hara[1,4], Akihiko Kudo[5], Hayato Kawakami[5], Yukio Saijoh[6], Masamichi Kurohmaru[1], Masami Kanai-Azuma[2,‡] and Yoshiakira Kanai[1,‡,§]

SUMMARY

Congenital biliary atresia is an incurable disease of newborn infants, of unknown genetic causes, that results in congenital deformation of the gallbladder and biliary duct system. Here, we show that during mouse organogenesis, insufficient SOX17 expression in the gallbladder and bile duct epithelia results in congenital biliary atresia and subsequent acute 'embryonic hepatitis', leading to perinatal death in ~95% of the *Sox17* heterozygote neonates in C57BL/6 (B6) background mice. During gallbladder and bile duct development, *Sox17* was expressed at the distal edge of the gallbladder primordium. In the *Sox17*$^{+/-}$ B6 embryos, gallbladder epithelia were hypoplastic, and some were detached from the luminal wall, leading to bile duct stenosis or atresia. The shredding of the gallbladder epithelia is probably caused by cell-autonomous defects in proliferation and maintenance of the *Sox17*$^{+/-}$ gallbladder/bile duct epithelia. Our results suggest that *Sox17* plays a dosage-dependent function in the morphogenesis and maturation of gallbladder and bile duct epithelia during the late-organogenic stages, highlighting a novel entry point to the understanding of the etiology and pathogenesis of human congenital biliary atresia.

KEY WORDS: *Sox17*, Haploinsufficiency, Biliary atresia, Hepatitis, Gallbladder, Bile duct, Mouse

INTRODUCTION

The biliary system in mice and humans transports bile from the liver to the duodenum and consists of the gallbladder, cystic duct, intra- and extrahepatic bile duct and common bile duct. Bile duct dysfunction in congenital biliary diseases and viral infection leads to the accumulation of bile in the liver, preventing excretion of detoxification products and liver injury (Zong and Stanger, 2011). Biliary atresia is a rare condition in newborn infants (Kohsaka et al., 2002; Mieli-Vergani and Vergani, 2009), characterized by inflammation in the bile ducts and liver due to the leakage of bile. Infants with biliary atresia are generally subdivided into two distinct clinical forms of the fetal/embryonic and perinatal/postnatal types (Schweizer, 1986; Desmet, 1992). The perinatal/postnatal type may be mainly caused by the virus infection and toxin exposure, leading to the apoptosis/necrosis of bile duct cells and subsequent inflammation/fibrosis around them. By contrast, the fetal/embryonic type (i.e. congenital biliary atresia), comprising one-third of patients, may be attributed to developmental errors in bile duct formation and morphogenesis by their genetic mutations. Studies in mouse models have identified signaling factors associated with congenital biliary atresia, such as Jagged1 (notch signaling; Kohsaka et al., 2002; Flynn et al., 2004) and Cryptic protein (nodal signaling; Bamford et al., 2000). However, the etiology and pathogenesis of the congenital (fetal/embryonic type) biliary atresia in both human and mice is not fully understood.

The intrahepatic and extrahepatic duct systems are derived from the liver and gallbladder primordium in the posterior-ventral foregut (Stainier, 2002; Zaret, 2008; Zaret and Grompe, 2008; Spence et al., 2009; Uemura et al., 2010). For the intrahepatic duct, cholangiocyte progenitors are derived from hepatocytes located adjacent to portal veins of the liver and are organized into ring structures (duct plates) around the portal vein branches. They form intrahepatic bile ducts that link the hepatocyte-lined bile canaliculi and the extrahepatic bile ducts (Shiojiri and Katayama, 1987; Clotman et al., 2002; Lemaigre, 2003; Carpentier et al., 2011). By contrast, the extrahepatic biliary structures (the gallbladder, cystic duct and extrahepatic ducts) are derived from the gallbladder primordium (Spence et al., 2009; Uemura et al., 2010; this study), which express SOX17, an SRY-related HMG box transcription factor that plays a conserved and vital function in definitive endoderm development in various vertebrate species (Tam et al., 2003).

In mice, *Sox17*-null embryos show a drastic reduction in endodermal cell population, and fail to develop beyond 10.5 days post coitum (dpc) (Kanai-Azuma et al., 2002). In the definitive endoderm, *Sox17* is transiently expressed during the initial phase of differentiation from mid-streak (7.0 dpc) to the early somite stages (Kanai-Azuma et al., 2002). Interestingly, during the early-somite (8.5 dpc) stages, *Sox17* is re-expressed in the posterior-ventral foregut, where the progenitors of the gallbladder/bile duct are found (Uemura et al., 2010) and is maintained in the gallbladder primordium during the perinatal period (this study). Cell-autonomous *Sox17* function in the foregut endoderm is required for the specification and differentiation of gallbladder/bile duct progenitors during foregut morphogenesis (Spence et al., 2009; Uemura et al., 2010). Despite the evolutionarily conserved

[1]Department of Veterinary Anatomy, The University of Tokyo, Yayoi 1-1-1, Bunkyo-ku, Tokyo 113-8657, Japan. [2]Center for Experimental Animal, Tokyo Medical and Dental University, Yushima 1-5-45, Bunkyo-ku, Tokyo 113-8510, Japan. [3]Department of Stem Cell Regulation, Medical Research Institute, Tokyo Medical and Dental University, Yushima 1-5-45, Bunkyo-ku, Tokyo 113-8510, Japan. [4]Division of Germ Cell Biology, National Institute for Basic Biology and Department of Basic Biology, School of Life Science, Graduate University for Advanced Studies (SOKENDAI), Okazaki, Aichi 444-8585, Japan. [5]Department of Anatomy, Kyorin University School of Medicine, Mitaka, Tokyo 181-8611, Japan. [6]Department of Neurobiology and Anatomy, The University of Utah, Salt Lake City, UT 84132-3401, USA.

*These authors contributed equally to this work
‡These authors contributed equally to this work
§Author for correspondence (aykanai@mail.ecc.u-tokyo.ac.jp)

Accepted 25 November 2012

SOX17 expression in gallbladder primordium and its derivatives among zebrafish (Shin et al., 2012), *Xenopus* (Zorn and Mason, 2001), mouse (Matsui et al., 2006; Uemura et al., 2010) and human (Cardinale et al., 2011; Carpino et al., 2012), it remains unclear how SOX17 activity in the gallbladder primordium is involved in the development and maturation of the gallbladder and bile duct system during the late organogenic stages. Moreover, the specification of the gallbladder primordium is regulated by several other factors such as *Foxf1* (Kalinichenko et al., 2002), *Hnf6* (*Onecut1* – Mouse Genome Informatics) (Clotman et al., 2002), *Hes1* (Sumazaki et al., 2004), *Hhex* (Hunter et al., 2007) and *Lgr4* (Yamashita et al., 2009). However, the molecular and cellular mechanisms that establish and maintain the gallbladder and bile duct system during the perinatal periods remain unknown.

In the present study, we showed that *Sox17* haploinsufficiency causes tissue-autonomous defects in the morphogenesis and maturation of gallbladder and bile duct epithelia in C57BL/6 (B6) background mice, leading to congenital biliary atresia and subsequent acute hepatitis in late fetal stages. This study adds new knowledge to our understanding of the pathogenesis of congenital biliary atresia and hepatitis.

MATERIALS AND METHODS

Animal care and use

All animal experiments in this study were performed in strict accordance with the Guidelines for Animal Use and Experimentation, as established by the University of Tokyo. The procedures were approved by the Institutional Animal Care and Use Committee of the Graduate School of Agricultural and Life Sciences in the University of Tokyo (approval ID: P11-501). Embryos at 13.5 to 17.5 dpc were obtained from pregnant wild-type females [C57BL/6 (B6) strain; Clea Japan] mated with *Sox17*$^{+/-}$ male mice (B6×129SvJ mixed background; Kanai-Azuma et al., 2002). *Sox17*$^{GFP/+}$ embryos (ICR background; 13.5 to 17.5 dpc; Kim et al., 2007) were also used in this study.

Histology, lectin histochemistry and immunohistochemistry

For whole-mount staining, the livers with gallbladder/bile duct tissues were fixed in 4% paraformaldehyde (PFA)-PBS for 6 hours at 4°C, and then washed with TBST. For permeabilization, all samples were dehydrated and stored in 70% methanol for several days. The samples were incubated with Rhodamine-labeled DBA lectin (10 μg/ml) or mouse anti-acetylated tubulin (1/100 dilution; Sigma) for 12 hours at 4°C.

For paraffin sections, the liver and gallbladder/bile duct tissues were fixed in 4% PFA-PBS for 12 hours at 4°C, dehydrated, embedded in paraffin and serially sectioned (5 μm in thickness). The 4% PFA-fixed frozen sections were also used (5-7 μm in thickness). All sections were subjected to conventional histological [Hematoxylin-Eosin (HE) and periodic acid Schiff (PAS) staining] and immunohistochemical staining.

For immunohistochemical staining, sections were incubated with mouse anti-acetylated tubulin (1/100 dilution; Sigma), mouse anti-BrdU (1/100 dilution; DakoCytomation), mouse anti-E-cadherin (1/250 dilution; BD Pharmingen), rabbit anti-GRP78 (1/500 dilution; Affinity Bioreagents), mouse anti-GFP (1/50 dilution; MBL), rabbit anti-HNF6 (1/50 dilution; Santa Cruz), rat anti-integrin β1 (1/50 dilution; Millipore), rabbit anti-laminin (1/250 dilution; ICN Pharmaceuticals), mouse anti-Ki67 (1/50 dilution; Leica), mouse anti-PCNA (1/5000 dilution; DACO), rabbit anti-SOX9 (1/250 dilution) (Kidokoro et al., 2005), rabbit anti-SOX17 (10 μg/ml) (Kanai et al., 1996), goat anti-SOX17 (1/100 dilution; R&D Systems) and mouse anti-ZO1 (1/100 dilution; Invitrogen) antibodies. Finally, the immunoreaction was visualized by biotin-conjugated secondary antibody in combination with an ABC Kit (Vector Laboratories) or by secondary antibodies conjugated with alkaline phosphatase/Alexa-488/594. After counterstaining with DAPI, the samples were analyzed under an Olympus fluorescent microscope (BX51N-34-FL2) and stereomicroscope (SZX16 plus U-LH100HG) systems and an Olympus FluoView confocal laser microscope (FV10i; Olympus, Japan).

For cell proliferation indices and morphometric data, PCNA/Ki67/BrdU-positive gallbladder epithelial cells and epithelial heights were separately estimated in the transverse sections at the levels of the largest duct diameter.

Organ culture

To analyze the tissue-autonomous phenotype of the *Sox17*$^{+/-}$ gallbladder/bile duct, we performed organ culture of the gallbladder primordium isolated at 13.5 dpc. Briefly, the gallbladder region without the proximal cystic duct was isolated from the fetal liver under a dissecting microscope at 13.5 dpc. The gallbladder primordia from the *Sox17*$^{+/-}$ and wild-type littermates were placed onto an ISOPORE membrane filter (Millipore), and then cultured in 10% fetal calf serum-DMEM (Sigma) at 37°C for 72 hours. In some explants, the gallbladder primordia were placed on gelatin-coated plates for the timecourse observation.

Transmission electron microscopy

Isolated liver and gallbladder/bile duct tissues were fixed in 2.5% glutaraldehyde/0.1 M phosphate buffer (PB) for 4 hours at 4°C. After washing with PBS, they were post-fixed in 1% OsO_4 in 0.1 M PB for 2 hours at 4°C. Then they were dehydrated and embedded in EPON812, and ultrathin sections were examined under a JEOL-1010 transmission electron microscope at 80 kV (Hara et al., 2009). In the electron micrographs (×5000) of the transverse sections at the levels of the largest duct diameter, the number of the primary cilia with the distinct basal body was counted and the total length of the luminal surface of the epithelial membrane was also measured to obtain the frequency of the primary cilia per each 100-μm apical cell surface.

RNA extraction, microarray and RT-PCR analyses

The *Sox17*$^{+/-}$ and wild-type liver tissues at 17.0 dpc were used for microarray expression analysis using the Affymetrix GeneChip system (Affymetrix). After the peripheral distal edge (one-third part) of each lobule was excised with a surgical scalpel under a dissecting microscope, the remaining proximal liver tissues (without any hepatic lesion) were used for subsequent RNA analysis, in order to make precise comparisons in the gene expression between the severe- and mild-phenotype samples. After total RNA was extracted using an RNeasy Mini Kit (Qiagen), double-stranded cDNA and biotin-labeled cRNA were synthesized using One-Cycle cDNA Synthesis and IVT Labeling kits (Affymetrix). Fragmented biotin-labeled cRNA (25 μg) was hybridized to the Affymetrix Mouse Expression Array MOE 430A for 16 hours at 45°C. The chips were analyzed using Microarray Suite version 5.0 (Affymetrix) in accordance with the manufacturer's standard protocols. Differential expression was defined as a difference of twofold or more in liver samples between *Sox17* heterozygote and wild type. The microarray data have been deposited in the Gene Expression Omnibus of NCBI (accession number: GSE33106).

For quantitative RT-PCR analysis, total RNA was extracted from the liver using Trizol reagent (Invitrogen). Each RNA sample was treated with DNase I, and then reverse transcribed using random primers with a Superscript-III cDNA synthesis kit (Invitrogen). A reverse transcriptase-free reaction was performed as a control. Real-time PCR was performed with TaqMan Universal PCR Master Mix (Applied Biosystems). Specific primers and fluorogenic probes for *Cxcl2* (Mm00436450_m1), *Cxcl1* (Mm00433859_m1), *Cxcl10* (Mm00445235_m1), *Ptgs2* (Mm00478374_m1), *Hspa1b* (Mm03038954_s1), *Hspa1a* (Mm01159846_s1), *Esm1* (Mm00469953), *Serpine1* (Mm00435860), *Jag1* (Mm00496902_m1), *Jag2* (Mm01325629_m1), *Notch1* (Mm00435249_m1), *Notch2* (Mm00803077_m1), *Hes1* (Mm01342805_m1), *Nodal* (Mm00443040_m1) and *Gapdh* (Taqman control reagents) were also purchased from Applied Biosystems. PCR was performed using an ABI Prism 7900HT sequence detector. Relative mRNA expression levels were calculated by the ΔΔCt analysis, using *Gapdh* (4352339E) mRNA for internal normalization.

Liver chemistry tests

Serum alanine aminotransferase (ALT) and alkaline phosphatase (ALP) were analyzed by SRL diagnostics (Tokyo, Japan). The intrahepatic bile acid levels were also determined using a Bile Acid L3K Assay Kit

Table 1. Viability of *Sox17*$^{+/-}$ pups on the C57BL/6 background*

Generation	+/+	+/–	Survival ratio (+/– / +/+)	Total number
N2	164	140	0.85	304
N3	190	155	0.82	345
N4	113	108	0.96	221
N5	85	11	0.13	96
N6	83	10	0.12	93
N7	69	8	0.12	77
N8	28	1	0.04	29

*Number of live neonates of each genotype in breedings between *Sox17*$^{+/-}$ males at each generation of backcross progeny from N2 [(C57BL/6↔129SvJ) F1↔C57BL/6] and wild-type females (C57BL/6).

(Diagnostic Chemicals) according to the manufacturer's directions (Bochkis et al., 2008).

Ink tracer experiment

The whole liver organ with the gallbladder/bile duct system and duodenum was isolated from wild-type or *Sox17*$^{+/-}$ embryos at 17.0 dpc. The red fluorescent ink (WA-TC 90; Tombo, Japan) was injected into the fetal gallbladder region at high pressures. The injected liver tissues were fixed with 4% PFA for 6 hours, and analyzed under an Olympus fluorescent microscope stereomicroscope system.

Statistical analysis

All quantitative data are represented as mean ± s.e.m. Data analysis was conducted with the graphics and statistics program PRISM v5.0 (GraphPad Software). Student's *t*-test or one-way ANOVA statistic was used to determine whether an overall difference existed between two groups or among more than three groups. Where differences existed, the Tukey test was also used to compare the value with every other values. A *P*-value of 0.05 or less was used to determine statistical significance for each analysis.

RESULTS

Sox17 haploinsufficiency results in defective perinatal development of both liver and gallbladder/bile ducts in B6 background mice

Perinatal lethality was found in ~90% of the *Sox17* heterozygote mutant pups after the N_5 generation of the backcross of *Sox17* heterozygote mutant mice (129/SvJ) onto the B6 background (Table 1). Pathological analyses of the *Sox17*$^{+/-}$ embryos in the $N_{7–8}$ generation in the B6 background (hereafter, *Sox17*$^{+/-}$ B6 or *Sox17*$^{+/-}$ embryo) revealed defects in the development of the liver and gallbladder/bile duct systems during the late-organogenic stages (Fig. 1). In 62.5% of the *Sox17*$^{+/-}$ B6 embryos ($N_{7–8}$), liver lobules showed peripheral degeneration with various degrees of severity at 17.5 dpc (55/88 embryos; Fig. 1A) based on gross anatomy. The peripheral degenerative areas were negative for PAS staining, which detects glycogen accumulation in healthy hepatocytes. Such peripheral degeneration was first detectable during 16.5-17.0 dpc, and the degenerative area rapidly expanded toward the central proximal region of the lobules. Moreover, liver weight was reduced significantly at 16.5 dpc in the *Sox17*$^{+/-}$ B6 embryos, compared with wild-type littermates (P<0.01; Fig. 1B).

In almost all *Sox17*$^{+/-}$ B6 embryos, the gallbladder region showed hypoplasia irrespective of whether hepatic lesions were present or not (Fig. 1C). Whole-mount dolichos biflorus agglutinin (DBA)-lectin staining revealed gallbladder hypoplasia at as early as 15.5 dpc (Fig. 1C). Ectopic extrahepatic ducts were also formed in the cystic duct region (21/22 in *Sox17*$^{+/-}$ versus 5/28 in wild type; Fig. 1C, white arrowheads).

Sox17$^{+/-}$ B6 embryos showed no histological abnormality in organs such as the lung, pancreas, esophagus, stomach, duodenum and intestine. In either ICR or 129SvJ/B6 ($N_{1–2}$) mixed backgrounds, the phenotypes of hepatitis and ectopic hepatic ducts

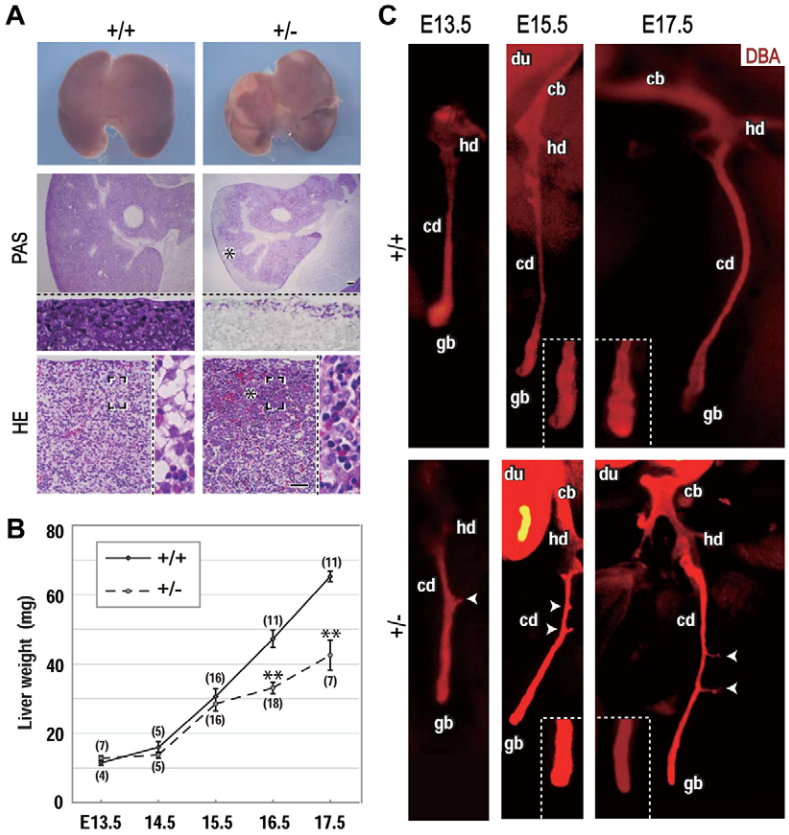

Fig. 1. Defective development of the liver and gallbladder/bile duct in *Sox17* heterozygote embryos in B6 background mice. (**A**,**B**) Gross-anatomical (upper panels in A) and histological [PAS staining (middle) and HE staining (lower panels in A)] images showing peripheral degeneration (asterisks and insets in A) of the liver lobules in *Sox17*$^{+/-}$ embryos at 17.5 dpc. In B, the line graph indicates significant reduction of liver weight in *Sox17*$^{+/-}$ embryos at 16.5 and 17.5 dpc compared with wild-type littermates (**P<0.01). Numbers in parentheses indicate the total number of the embryos used in each group. Error bars represent s.e.m. (**C**) Whole-mount DBA staining shows hypoplastic gallbladder (gb, insets) and ectopic formation of extrahepatic ducts (white arrowheads) in *Sox17*$^{+/-}$ embryos during 13.5 to 17.5 dpc. cb, common bile duct; cd, cystic duct; du, duodenum; gb, gallbladder; hd, extrahepatic duct. Scale bar: 50 μm.

Table 2. Top 20 of the 59 upregulated genes in *Sox17*$^{+/-}$ livers (B6) at 17.0 dpc*

Description	Gene	Fold change‡ Severe	(Mild)
Endothelial cell-specific molecule 1	*Esm1*	115.7	(10.1)
Chemokine (C-X-C motif) ligand 10	*Cxcl10*	49.0	(6.4)
Heat shock protein 1A	*Hspa1a*	28.9	(14.2)
Heat shock protein 1B	*Hspa1b*	28.8	(17.5)
Chemokine (C-X-C motif) ligand 2	*Cxcl2*	26.6	(5.1)
Patched domain containing 3	*Ptchd3*	24.7	(5.6)
Serine (or cysteine) peptidase inhibitor, clade E, member 1	*Serpine1*	24.2	(158.7)
Kallikrein 1-related peptidase b24	*Klk1b24*	21.2	(5.1)
Phosphatidylinositol-4-phosphate 5-kinase, type 1 alpha	*Pip5k1a*	20.2	(2.0)
Hepcidin antimicrobial peptide	*Hamp*	19.2	(4.3)
Predicted gene 6297	*Gm6297*	13.0	(3.8)
Chemokine (C-X-C motif) ligand 1	*Cxcl1*	12.4	(4.3)
Procollagen lysine, 2-oxoglutarate 5-dioxygenase 2	*Plod2*	11.9	(4.0)
Chondroitin sulfate synthase 3	*Chsy3*	9.2	(3.3)
Activating transcription factor 3	*Atf3*	8.7	(6.6)
RIKEN cDNA 4930583H14 gene (mitochondria localized glutamic acid rich protein)	*4930583H14Rik* (*Mgarp*)	8.4	(3.4)
Ankyrin repeat domain 37	*Ankrd37*	8.0	(7.8)
Potassium voltage-gated channel, Isk-related subfamily, gene 3	*Kcne3*	7.9	(5.9)
Family with sequence similarity 184, member A	*Fam184a*	6.9	(6.5)
Chemokine (C-C motif) ligand 2	*Ccl2*	5.9	(3.9)

*Microarray expression analyses were performed using the cDNA samples collected from the central proximal region of the liver lobules in which any degenerative area was detected based on gross anatomy, even in the severe group. In the mild group, the cDNA samples were also prepared from the proximal regions of the liver lobules (the livers in the mild group were normal without any hepatitis phenotype at 17.0 dpc).
‡The fold change represents the difference in expression levels in livers between *Sox17*$^{+/-}$ and wild-type littermates. Differential expression was defined as a difference of twofold or more.

in *Sox17*$^{+/-}$ embryos were considerably milder than those in the B6 background, although the gallbladder hypoplasia became evident in almost all of the samples in the adult stage (supplementary material Fig. S1A,B). As anti-SOX17 signal intensities in gallbladder primordia appear to be lower in *Sox17*$^{+/-}$ embryos than those in wild-type littermates in both ICR and B6 backgrounds (supplementary material Fig. S1C), *Sox17* haploinsufficiency (i.e. a dosage-dependent effect) causes aberrant development of the liver and gallbladder/bile duct by the perinatal stage on the B6 background.

Perinatal hepatic inflammation and cholestasis in the *Sox17*$^{+/-}$ (B6) liver

To understand the molecular basis of liver phenotypes, we performed microarray analyses of the isolated liver tissues of the *Sox17*$^{+/-}$ and wild-type littermates (each cDNA sample was prepared from the *Sox17*$^{+/-}$ embryo with or without gross-anatomical hepatic lesions as severe- or mild-phenotype group, respectively). Microarray array analysis identified 59 upregulated genes (Table 2) and 17 downregulated genes (supplementary material Table S1) in *Sox17*$^{+/-}$ livers compared with wild-type livers. Among the top 20 upregulated genes, expression of inflammatory cytokines (e.g. *Cxcl10*, *Cxcl2* and *Cxcl1*) and stress-induced heat-shock protein markers (*Hspa1a* and *Hspa1b*) was elevated in *Sox17*$^{+/-}$ livers at 17.0 dpc, compared with wild-type littermates. The qPCR analyses of the *Sox17*$^{+/-}$ livers at 17.0 dpc [the earliest stage at which the degenerative region in some *Sox17*$^{+/-}$ livers (i.e. severe-phenotype group) was detected] confirmed the significantly increased expression of various inflammatory cytokines and hepatotoxic marker genes (*Cxcl1*, *Cxcl2*, *Cxcl10*, *Ptgs2*, *Esm1* and *Serpine1*) in a severity-dependent manner (Fig. 2A). Interestingly, such increased expression of inflammatory cytokines was not detected in the *Sox17*$^{+/-}$ livers at 15.5 dpc, just before the first biliary excretion into the fetal duodenum (supplementary material Fig. S2). Moreover, the levels of serum ALT and ALP (two hepatitis markers) were significantly elevated in *Sox17*$^{+/-}$ embryos compared with wild-type littermates at 17.0 dpc (Fig. 2B, upper two graphs). The intrahepatic level of bile acids was also significantly elevated in *Sox17*$^{+/-}$ livers (Fig. 2B, lowest graph).

Because elevated levels of intrahepatic bile acid level is known to cause endoplasmic reticulum (ER) stress in livers (Bernstein et al., 1999; Bochkis et al., 2008), the expression pattern of GRP78 (an ER stress marker) was also examined in developing *Sox17*$^{+/-}$ livers. GRP78 expression was upregulated in hepatocytes surrounding the PAS-negative degenerative areas in the *Sox17*$^{+/-}$ livers (Fig. 2C; supplementary material Fig. S3). Ultrastructural analysis also confirmed the characteristic ER enlargement in the cytoplasmic region facing the bile canaliculi in the hepatocytes around the degenerative region (Fig. 2D). Taken together, these data indicate the development of cholestasis and perinatal onset of hepatic inflammation in the *Sox17*$^{+/-}$ B6 livers during 16.5 to 17.5 dpc.

SOX17 is highly expressed in proliferating epithelial cells of the gallbladder primordium, but not in fetal hepatocytes during mid- and late-organogenic stages

To determine the cause of the acute hepatitis in the *Sox17*$^{+/-}$ B6 embryos, the sites of SOX17 expression in the liver and gallbladder/bile duct system were examined by immunostaining (ICR background) (Uemura et al., 2010) or a *Sox17*-GFP reporter line (ICR background; Kim et al., 2007). At 13.5 to 17.5 dpc, no SOX17 was detected in fetal hepatocytes in the lobules (Fig. 3A,B). By contrast, strong expression of SOX17 was observed in the gallbladder epithelia, even in late-organogenic stage embryos (13.5-16.5 dpc) ('gb' in Fig. 3C,D). SOX17 was also detected in the cystic duct epithelia ('cd' in Fig. 3C,D), but not in the common bile duct and extra- and intrahepatic ducts ('hd' in Fig. 3C,D; data not shown). The vascular endothelial cells and

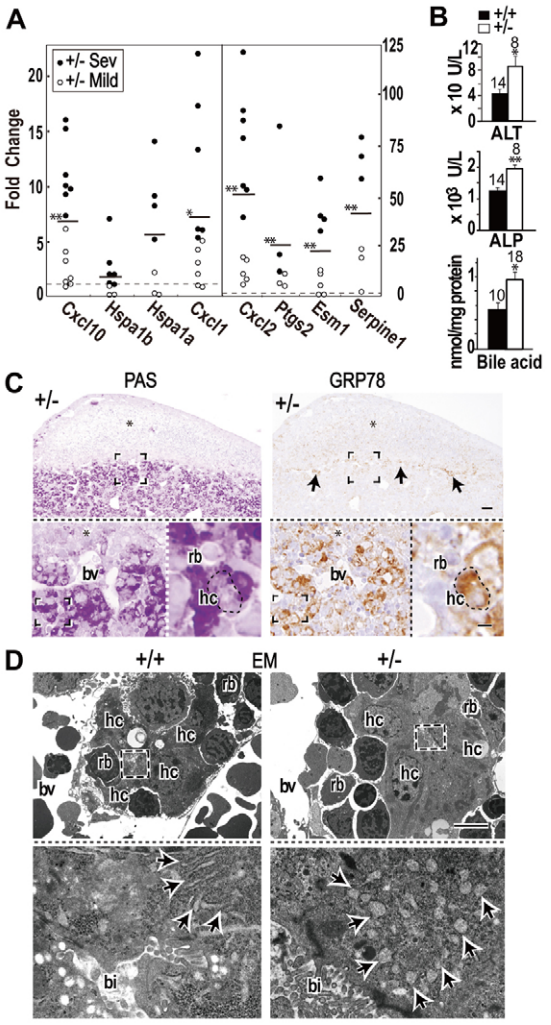

Fig. 2. Hepatic inflammation with elevated bile acid levels and endoplasmic reticulum stress of hepatocytes in fetal *Sox17*$^{+/-}$ B6 livers. (**A**) Real-time RT-PCR analysis showing elevated expression levels of several inflammatory cytokine markers in *Sox17*$^{+/-}$ B6 livers at 17.0 dpc. The vertical axis represents fold changes in the expression level of each liver sample relative to those of wild-type livers (the mean value was set as 1). Filled (severe) and unfilled (mild) circles indicate *Sox17*$^{+/-}$ liver samples with and without any gross-anatomical lesions, respectively. The bars show mean values of all (severe and mild) samples, whereas asterisks on the bar indicate significant differences compared with wild-type livers (*P<0.05, **P<0.01). (**B**) Biochemical data showing significantly elevated levels of serum ALT, serum ALP and intrahepatic bile acids in *Sox17*$^{+/-}$ livers compared with wild-type livers. Error bars represent s.e.m. (**C**) PAS (red) and anti-GRP78 immunostaining (brown) of two consecutive sections, showing GRP78-positive signals in the hepatocytes around the degenerating peripheral region of *Sox17*$^{+/-}$ liver lobules (arrows). Asterisks indicate the PAS-negative region including the damaged hepatocytes. (**D**) Electron microscopic images showing enlargement of rough ER (arrows) in *Sox17*$^{+/-}$ hepatocytes. Each dashed rectangle indicates the area highly magnified in the adjacent panel. bi, bile canaliculus; bv, blood vessel; hc, hepatocyte, rb, red blood (hematopoietic) cells. Scale bars: 50 μm in upper panels in C; 5 μm in lower right inset of C and in D.

hematopoietic cells were positive for SOX17 and express SOX17-GFP. Anti-proliferating cell nuclear antigen (PCNA) staining revealed high proliferative activities of SOX17-positive bile duct epithelial cells in the distal region of the developing gallbladder/bile duct primordium at 13.5 and later stages (Fig. 3E,F; supplementary material Fig. S4).

Hypoplasia and deciduation of gallbladder epithelia lead to bile duct stenosis and atresia in the *Sox17*$^{+/-}$ B6 embryos

Histological analysis clearly revealed that the phenotype of the gallbladder of *Sox17*$^{+/-}$ (B6) embryos was associated with the hypoplasia of the gallbladder epithelium, which can be detected as early as 15.5–16.5 dpc (Fig. 4A). In wild-type embryos, the gallbladder epithelium acquired a columnar architecture at 15.5 to 16.5 dpc, forming a pseudostratified columnar epithelium in the gallbladder by 17.5 dpc (Fig. 4A,B, left-hand panels). By contrast, *Sox17*$^{+/-}$ gallbladder formed hypotrophic, single-layered cuboidal epithelium with no epithelial fold formation (Fig. 4A,B, right-hand panels). Morphometric analysis showed that the epithelial height in *Sox17*$^{+/-}$ gallbladder epithelium was reduced compared with wild-type littermates (25.8±1.0 μm in nine wild-type embryos versus 17.4±0.6 μm in 14 *Sox17*$^{+/-}$ embryos at 17.5 dpc, P<0.01). Ultrastructural examination revealed the presence of a monolayer epithelium in the *Sox17*$^{+/-}$ gallbladder with an underdeveloped reticular lamina layer in the basal lamina lining the outer wall of the duct (Fig. 4B, lower insets). Although some epithelial cells were detached from the adjacent epithelial cells (Fig. 4A,B, arrows; also see Fig. 5A,B), most epithelial cells of the gallbladder showed no appreciable ultrastructural abnormalities based on transmission electron microscopy.

A comparison of the PCNA-positive indices in the gallbladder epithelial cells (i.e. bile duct cells at the largest diameter of the distal edge) showed that the gallbladder epithelia of wild-type embryos, which was high at 15.5 dpc, dropped significantly (P<0.01, Tukey test) by 16.5 dpc (Fig. 4C). In *Sox17*$^{+/-}$ gallbladder epithelia at 15.5 and 16.5 dpc, the PCNA-positive indices were significantly (P<0.01) reduced compared with the wild-type counterparts (Fig. 4C). Both Ki-67- and BrdU-labeling indices were also shown to be significantly reduced in *Sox17*$^{+/-}$ gallbladder epithelia at 15.5 dpc (supplementary material Fig. S5).

Interestingly, the gallbladder epithelial cells were occasionally detached from the gallbladder wall (Fig. 5A,B), and then accumulated inside the lumina of the cystic and extrahepatic ducts in the *Sox17*$^{+/-}$ B6 embryos (Fig. 5A-E). Anti-HNF6 and DBA-lectin staining (the markers for bile duct epithelial cells) confirmed that these luminal decidual cells were positive for both HNF6 and DBA staining (Fig. 5A). Anti-E-cadherin staining revealed no appreciable defects in the *Sox17*$^{+/-}$ gallbladder epithelia (Fig. 5B). These luminal decidual cells clearly caused the stenosis and atresia in the cystic and extrahepatic ducts to varying degrees (Fig. 5C-E, arrowheads). Ultrastructural analysis revealed a close connection between bile duct epithelial cells and the luminal decidual cells via the apical surface (C1, C3 in Fig. 5C). However, necrotic cell death was observed in several decidual cells located in the center of the laminated epithelial plug (C2 in Fig. 5C). In cases of complete biliary atresia, DBA-positive materials filled the lumina of extrahepatic ducts (Fig. 5D,E, right-hand panels). Taken together, these findings suggest that the defective proliferation and maintenance of the *Sox17*$^{+/-}$ gallbladder/bile duct epithelia partially caused their detachment from the duct wall in the lumen, which secondarily leads to bile duct stenosis and atresia in the cystic and extrahepatic ducts.

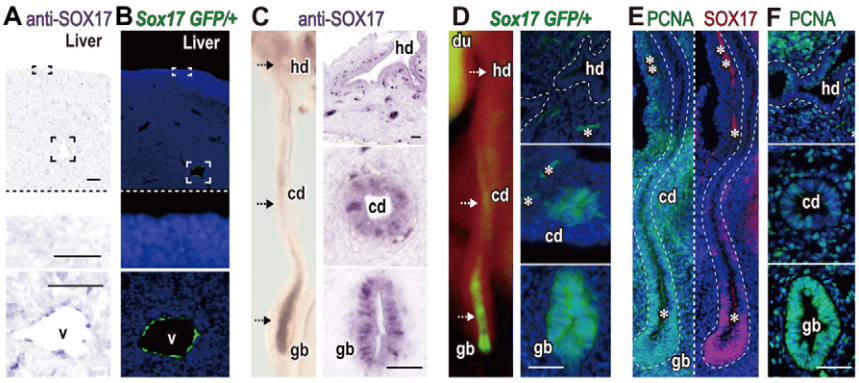

Fig. 3. SOX17 is highly expressed in proliferating gallbladder epithelia, but not in hepatocytes during the late-organogenic stages. (**A-F**) Anti-SOX17 (purple in A and C, red fluorescence in E) and anti-PCNA (green fluorescence in E and F) immunostaining of wild-type embryos and GFP fluorescence images of *Sox17*$^{GFP/+}$ embryos (green fluorescence in B and D) at 13.5 dpc (E) and 16.5 dpc (A-D,F) showing SOX17 expression sites in developing liver (A,B) and gallbladder/bile duct (C-F). In A and B, the two lower insets indicate higher-magnified images of the surface (upper) and proximal (lower) regions of the liver lobules surrounded by the broken rectangles in the top panels, respectively. In C and D, left panels show SOX17 expression in whole-mount images of the gallbladder/bile-duct, whereas right panels display the transverse section images corresponding to the plane of the dashed lines at the levels of extrahepatic duct, cystic duct and gallbladder. (E,F) Anti-SOX17 (red) and anti-PCNA (green) double-immunostaining of the sagittal section (E) and anti-PCNA staining of the transverse section (F) of the gallbladder/bile-duct (DAPI, blue). Asterisk indicates non-specific fluorescence. cd, cystic duct; hd, extrahepatic duct; gb, gallbladder; v, blood vessel. Scale bars: 50 μm.

In contrast to the abnormal anatomy of gallbladder and extrahepatic bile ducts, SOX9-positive intrahepatic bile ducts were formed properly around the portal vein of the proximal region of the liver lobules even in livers with lesions (Fig. 6A). A fluorescent ink-tracer experiment did not reveal any defects in intrahepatic biliary trees at 17.0 dpc (3/3 *Sox17*$^{+/-}$ embryos; Fig. 6B).

As for notch/nodal signaling (Bamford et al., 2000; Kohsaka et al., 2002; Flynn et al., 2004), no significant changes in the expression levels of *Jag1*, *Jag2*, *Notch1*, *Notch2*, *Hes1* and *Nodal* in the gallbladder/bile ducts primordium were detected between wild-type and *Sox17*$^{+/-}$ embryos (supplementary material Fig. S6). As for the left-right laterality and cilia formation [which were speculated to be closely associated with congenital biliary atresia in humans (Nakanuma et al., 2010; Chu et al., 2012)], no appreciable defects in both laterality (data not shown) and cilia formation in gallbladder/bile ducts (supplementary material Fig. S7) were observed in *Sox17*$^{+/-}$ embryos at 15.5-16.5 dpc. The frequencies of the primary cilia in the *Sox17*$^{+/-}$ gallbladder epithelia appear to be increased, rather than reduced, compared with those in wild type (supplementary material Fig. S7D).

Defective elongation and shredding of epithelial cells in *Sox17*$^{+/-}$ bile duct epithelia in the organ culture using gallbladder primordium

To study the cellular events leading to defects in the *Sox17*$^{+/-}$ gallbladder/bile duct epithelium, we cultured gallbladder primordia of 13.5 dpc *Sox17*$^{+/-}$ and wild-type embryos, and then analyzed the elongation and morphogenesis of the duct structure (Fig. 7A,B). During *in vitro* culture, the wild-type gallbladder primordium elongated in a distal-proximal manner to form the tubular structure [39/45 explants (6/45: no outgrowth); Fig. 7B, left-hand panels]. A considerable regionalized distribution of PCNA-positive epithelial cells was found in the distal region of elongated wild-type gallbladder explants (11/11 explants; white arrow indicates proximal

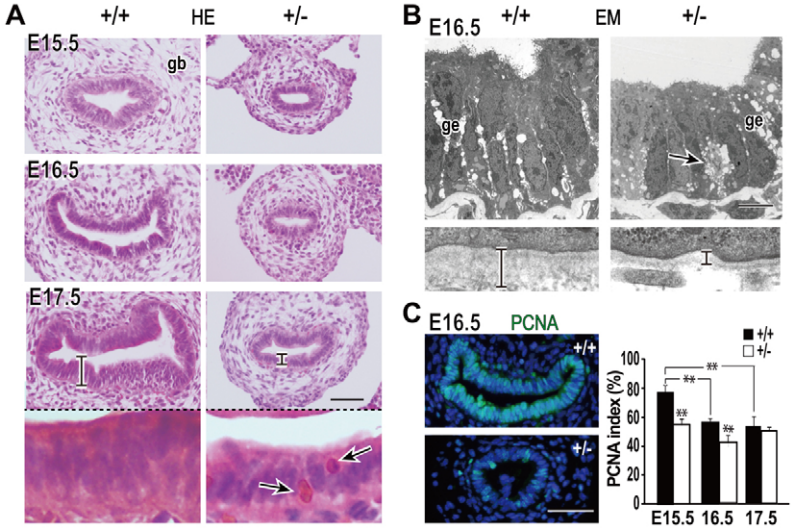

Fig. 4. Hypoplasia of *Sox17*$^{+/-}$ gallbladder epithelium during late-organogenic stages. (**A**,**B**) Light (A; HE staining) and electron (B) microscopic images of gallbladder epithelia (transverse sections at the levels of maximum diameter), showing hypoplasia of *Sox17*$^{+/-}$ gallbladders at 15.5 to 17.5 dpc. Gallbladder epithelial cells showed defective maturation (vertical bars indicate epithelial cell height in A and basal lamina thickness in B) in *Sox17*$^{+/-}$ embryos. Arrows in A and B indicate presumptive decidual cells within the gallbladder epithelia. (**C**) Anti-PCNA immunofluorescence images (left panels) and quantitative data (right graph) showing significant reductions in the PCNA-positive index (**P<0.01 at 15.5 and 16.5 dpc) in *Sox17*$^{+/-}$ gallbladder epithelia (n=10 embryos in each bar). Error bars represent s.e.m. gb, gallbladder; ge, gallbladder epithelial cells. Scale bars: 50 μm in A,C; 5 μm in B.

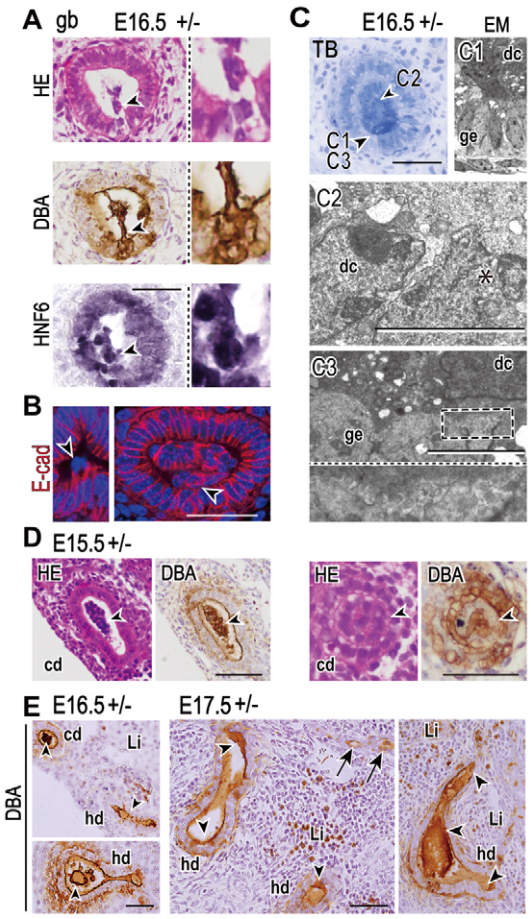

Fig. 5. Epithelail cell deciduation in the gallbladder, and biliary obstruction in the cystic duct and extrahepatic duct regions of *Sox17*$^{+/-}$ embryos. (**A-E**) Light (HE, DBA-lectin, anti-HNF6 and anti-E-cadherin (E-cad) staining) and electron microscopic images showing epithelial cell deciduation in the gallbladder (A-C) and luminal sloughed cells/cell debris in the cystic and extrahepatic ducts (arrowheads in D,E). Sloughed epithelial cells are positive for DBA lectin staining and anti-HNF6/E-cad immunostaining (arrowheads in A,B). In the gallbladder/cystic duct regions, luminal decidual cells can occupy the luminal space (right panel in B; and C). In the center of the obstruction region, the decidual cells undergo necrosis (asterisk in C2), whereas several outer decidual cells are tightly connected to the luminal cell surface of the bile duct epithelia (C3). In the cystic duct and extrahepatic duct regions at 15.5-17.5 dpc, the decidual cells are frequently found in the lumen (arrowheads in D and left panels of E), resulting in biliary atresia in the extrahepatic ducts (arrowheads in two right panels of E; the arrows indicate intrahepatic bile ducts). cd, cystic duct; dc, decidual cells in the lumen; gb, gallbladder; hd, extrahepatic duct; Li, liver parenchyma. Scale bars: 50 μm (except for 5 μm in C2,C3).

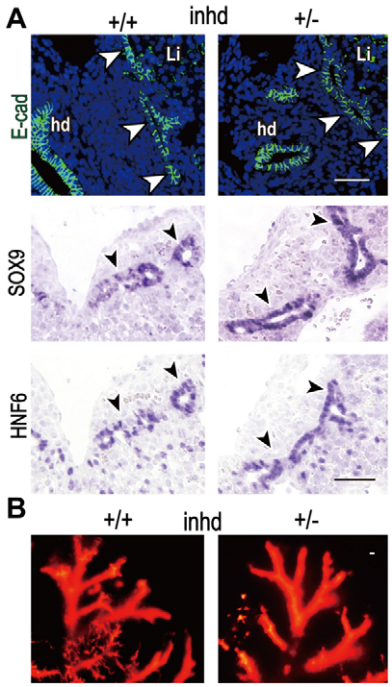

Fig. 6. No appreciable defects in the formation and branching of intrahepatic biliary trees in fetal *Sox17*$^{+/-}$ livers. (**A**,**B**) Anti-E-cad (green fluorescence), SOX9 and HNF6 (purple) immunostaining (A) and a tracer experiment by injecting fluorescent ink into the gallbladder under high pressure (red fluorescence; B) revealed proper formation of the intrahepatic duct tree (arrowheads), even in *Sox17*$^{+/-}$ livers with gross-anatomical hepatic lesions at 17.0 dpc. hd, extrahepatic duct; inhd, intrahepatic bile duct; Li, liver parenchyma. Scale bars: 50 μm.

side in Fig. 7C). By contrast, *Sox17*$^{+/-}$ gallbladder primordium formed a balloon-like cystic structure and lacked directional elongation [33/39 explants (6/39: no outgrowth); Fig. 7B, right-hand panels; supplementary material Fig. S8]. There was also no regionalization of PCNA-positive cells in the balloon-like structure formed in the *Sox17*$^{+/-}$ explants (11/11 explants; Fig. 7C). In 4/14 *Sox17*$^{+/-}$ explants, cellular debris was found inside the lumen of the balloon-like cyst (Fig. 7C, white arrowheads), and the neighboring epithelial lining displayed patchy laminin (Fig. 7C, white dashed arrow). The wild-type gallbladder explants showed a well-developed pseudostratified columnar epithelium with the epithelial folds (Fig. 7D, left-hand panels), whereas *Sox17*$^{+/-}$ gallbladder epithelium was hypotrophic and remained as a monolayer of low cuboidal cell (epithelial height=30.0±1.5 μm in seven wild-type explants versus 10.4±1.1 μm in six *Sox17*$^{+/-}$ explants, $P<0.01$; Fig. 7D). Although expression of E-cadherin and ZO-1 was unaffected, integrin β1 [a cell adhesion receptor to the extracellular matrix (ECM)] was reduced in *Sox17*$^{+/-}$ gallbladder explants compared with wild-type explants (Fig. 7E). Taken together, these data suggest that reduced *Sox17* activity in gallbladder epithelium results in the loss of regionalized cell proliferation, the defective maturation of epithelial structure and the failure to form tubular structures in a tissue-autonomous manner. These explants display a phenocopy of the hypoplasia and deciduation of bile duct epithelia of *Sox17*$^{+/-}$ B6 embryos.

DISCUSSION

After transient expression of *Sox17* in the definitive endoderm in the early stages (Kanai-Azuma et al., 2002), *Sox17* expression becomes re-upregulated in the most-posterior and lateral domains of the ventral foregut endoderm during the 9- to 10-somite stages, in which the gallbladder/bile duct primordium is initially specified (Uemura et al., 2010). A complete loss of SOX17 activity leads to the failure of gallbladder formation and changes in the molecular phenotype (loss of DBA and HNF6 expression) of bile duct cells (Spence et al., 2009; Uemura et al., 2010), indicating a crucial role of SOX17 activity in gallbladder/bile duct specification during the

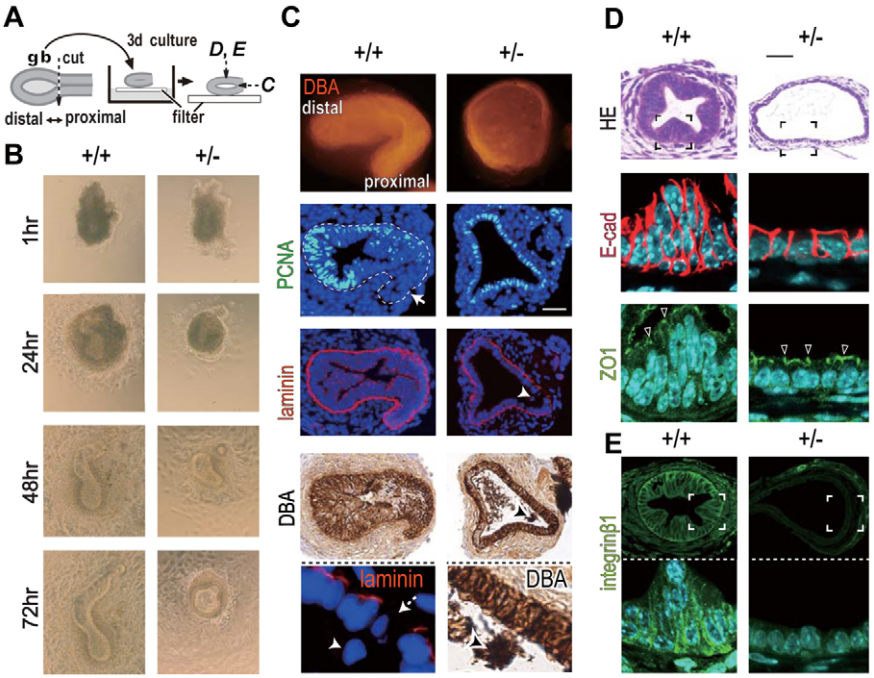

Fig. 7. Reduced elongation, non-polarized proliferation, and shredding of epithelial cells of *Sox17*$^{+/-}$ gallbladder primordium *in vitro*. (**A**,**B**) Schematic (A) and phase-contrast images of the timecourse (B) of a 3-day organ culture of gallbladder primordium initiated at 13.5 dpc. The dashed arrows show the sectioning planes corresponding to C, D and E. (**C-E**) DBA-stained whole-mount images (horizontal view; C); anti-PCNA-, anti-laminin-, and DBA-stained section images (horizontal section; C), HE- and anti-E-cad/anti-ZO1-stained images (transverse sections; D); and anti-integrin β1-stained images (transverse sections; E) of *Sox17*$^{+/-}$ and wild-type explants initiated at 13.5 dpc (3-day culture). The wild-type gallbladder explants showed polarized elongation of the ductural structure (B), polarized distribution of PCNA-positive epithelial cells along the distal-proximal axis (white unbroken arrow: PCNA-negative proximal region in C), and epithelial fold formation (D) in the developing gallbladder primordium *in vitro*. By contrast, *Sox17*$^{+/-}$ explants displayed a non-polarized balloon-like structure surrounded by a single thin epithelial cell layer (B-E), non-polarized distribution of PCNA-positive epithelial cells (C), a partial lack of anti-lamimin signals with the decidual epithelial cells (dashed arrow and filled arrowhead in C), and reduced anti-integrin β1 signals at the basal surface of the epithelial cells (E). The bottom panel in C show the *Sox17*$^{+/-}$ decidual epithelial cells indicated by arrowheads in the upper panels. Scale bar: 50 μm.

initial phase of ventral foregut morphogenesis. In this study, we extended the investigation to a more advanced stage of organogenesis of the gallbladder and bile duct in *Sox17*$^{+/-}$ mutant on a B6 background and showed that SOX17 is required for the proper morphogenesis and maintenance of gallbladder and bile duct epithelia during fetal and perinatal life.

Genetic background has been shown to influence phenotype and survival of mutants in a variety of mouse disease models (Doetschman, 1999). The *Sox17*$^{+/-}$ pups in the N4-N5 generation on a B6 background rapidly reduced the survival rate, which appeared to be accompanied by increased ratios of embryonic hepatitis (Table 1; supplementary material Fig. S1A). As any direct descendant of *Sox17*$^{+/-}$ pups was obtained from the *Sox17*$^{+/-}$ N_9 males (data not shown), the lethal phenotype in *Sox17*$^{+/-}$ mutants might be affected by multiple (two or more) modifier genes (including polymorphic repetitive sequences involved in their expression levels) in the B6 background.

SOX17 is expressed in the actively proliferating epithelial cells in the distal region of the gallbladder primordium to sustain the growth of the ductal organ. Reduced *Sox17* activity is closely associated with reduced proliferation and luminal deciduation of the gallbladder epithelial cells, resulting in bile duct atresia and stenosis and secondarily induced embryonic hepatitis. Although the similarities in these phenotypes of the *Sox17*$^{+/-}$ mouse model with the etiopathogenesis of human biliary atresia remain unclear, the cell-autonomous injury of the bile duct epithelia seen in the *Sox17*$^{+/-}$ gallbladder/bile duct primordium is widely accepted as one of the direct causes of the congenital biliary atresia in humans (Nakamura et al., 2010). This *Sox17* heterozygous mutant on a B6 background therefore provides a clinically relevant experimental model for congenital biliary atresia and embryonic hepatitis elicited secondarily by malformations of extrahepatic bile duct.

It is well known that SOXF factors (including SOX17) are involved in the expression of the fibronectin 1 (*Fn1*) (Shirai et al., 2005) and laminin, alpha 1 (*Lama1*) (Niimi et al., 2004) genes encoding constituents of the basement membrane. Moreover, previous studies have demonstrated that SOX17 functions as a transcriptional regulator in the basal lamina formation of the extra-embryonic endoderm (Shimoda et al., 2007) and parietal endoderm (Artus et al., 2011). The present histological observations revealed poorly developed reticular lamina of the basement membrane and reduced expression of integrin β1 signals in the *Sox17*$^{+/-}$ gallbladder epithelia (Fig. 4B; Fig. 7C,E). However, our culture experiments using the *Sox17*$^{+/-}$ gallbladder explants embedded in Matrigel (basement membrane matrix) revealed that exogenous supply of basement membrane matrix could rescue neither defective epithelial maturation (i.e. epithelial fold formation) nor polarized cell proliferation in *Sox17*$^{+/-}$ gallbladder explants, showing the balloon-like cystic structure with a single columnar epithelial layer in almost of the explants embedded in Matrigel (see supplementary material Fig. S9). Recently, SOX17 was also shown to repress the expression of *Rhou*, a Cdc42-related atypical Rho GTPase gene, which is a novel factor

that plays a role in maintaining epithelial architecture in the foregut endoderm in mouse early-somite-stage embryos (Loebel et al., 2011). These findings raise the possibility that cell-autonomous defects in Rho signaling and cell adhesion with the ECM might cause luminal deciduation of the gallbladder epithelial cells into the bile duct lumen in *Sox17*$^{+/-}$ embryos.

In infants and children with biliary atresia, 10~20% of the fetal/embryonic type demonstrate left-right laterality defects, and some patients with the mutation in *PKHD1*, encoding the ciliary protein fibrocystin, are closely correlated with a ciliopathy with clinical features that resemble biliary atresia (Nakamura et al., 2010; Hartley et al., 2011). Moreover, cilia structure and distribution within bile ducts were previously shown to be affected in the specimens of human biliary atresia: shorter, abnormal orientation, and less abundant cilia in the biliary atresia specimens (Chu et al., 2012). These findings raise a possible association of the reduced *Sox17* activity in the gallbladder primordium with the ciliopathy associated with congenital biliary atresia. However, the *Sox17*$^{+/-}$ embryos and surviving adults did not show any defects in left-right laterality (data not shown), despite the defective establishment of left-right asymmetry in *Sox17* null-embryos at early-somite stages (Viotti et al., 2012; Saund et al., 2012). Moreover, in the *Sox17*$^{+/-}$ gallbladder primordia, cilia formation in the gallbladder/bile duct region appears not to be affected, and the relative number of primary cilia on the apical surface appears to be increased, rather than decreased, in the *Sox17*$^{+/-}$ gallbladder epithelia (supplementary material Fig. S7). This is also consistent with no defects in cilia structure/function in the node of *Sox17*-null embryos (Saund et al., 2012). However, further studies are needed to understand cilia function and downstream signals in the gallbladder/ bile duct system and their direct association with the biliary atresia in both mouse models and humans.

Based on the present histopathological and RNA analyses of *Sox17*$^{+/-}$ livers, it is likely that bile duct stenosis and atresia of the decidual gallbladder epithelia are closely associated with bile acid cholestasis in the intrahepatic region, resulting in hepatic ER stress and subsequent onset of embryonic hepatitis (see Fig. 2) (Bernstein et al., 1999). Interestingly, the peripheral hepatocytes were most sensitive to the embryonic hepatitis in the *Sox17*$^{+/-}$ livers (Fig. 2C; supplementary material Fig. S3). This may be associated with the recent study showing that the morphogenesis and proliferation of the hepatocytes occur more actively in the peripheral region than in the central region of each liver lobule in the late-organogenic-stage embryos (Onitsuka et al., 2010). It is also possible that hepatocytes in the periphery might respond first in an inflammatory response through the vasculatures, because blood flows from the periphery toward the center of each liver lobule.

Our immunohistochemical analysis revealed that *Sox17* was expressed in the vascular endothelial and hematopoietic cell lineages in livers, but not in fetal hepatocytes (Fig. 3A,B). Moreover, we could not detect any defects in the vascular endothelial and hematopoietic cells in fetal *Sox17*$^{+/-}$ livers (see supplementary material Figs S10, S11), consistent with previous reports based on co-expression patterns and redundant functions of SOX17 with SOX7 and SOX18 in these two cell lineages (Matsui et al., 2006; Sakamoto et al., 2007; Cermenati et al., 2008; Hosking et al., 2009; Francois et al., 2010; Serrano et al., 2010; He et al., 2011). Because no appreciable defects in early differentiation of the hepatocyte lineage could be detected in *Sox17*-null foregut endoderm (Kanai-Azuma et al., 2002; Uemura et al., 2010), these data suggest that extrahepatic duct atresia of these decidual gallbladder epithelia contributes at least partially to hepatocyte ER stress and subsequent acute onset of hepatitis in a tissue-non-autonomous fashion. However, we cannot completely rule out a potential contribution of tissue-autonomous SOX17 activity in certain hepatic multipotent stem/progenitor cells that only weakly or transiently express SOX17 in a developmental-stage-dependent manner (Cardinale et al., 2011; Okada et al., 2012; Pfister et al., 2011).

In the model we propose, SOX17 maintains the epithelial architecture of the gallbladder/cystic duct system through their progenitor cells located in the distal region of the gallbladder epithelia. The SOX17-positive gallbladder/cystic-duct progenitor cells proliferate and consequently contribute to the epithelial architecture of the gallbladder and cystic duct system during late-organogenic stages. During the polarized proliferation and elongation processes of the gallbladder and cystic duct along the proximodistal axis, some *Sox17*$^{+/-}$ epithelial cells have certain defects in the maturation of epithelial characteristics, becoming detached from the epithelial walls into the lumen (i.e. injured bile duct epithelial wall), which consequently causes congenital biliary atresia in extrahepatic ducts of *Sox17*$^{+/-}$ B6 embryos. It is likely that, just after the first biliary excretion into the fetal duodenum (16.5 dpc), such congenital biliary atresia by luminal epithelia deciduation induces cholestasis with elevated levels of both intrahepatic bile acids and hepatic ER stress, subsequently leading to acute hepatic inflammation around the perinatal stage of the *Sox17*$^{+/-}$ embryos. In *Sox17*$^{+/-}$ embryos, the positive response to the cholestasis might lead to ectopic formation of extrahepatic ducts in the cystic ducts. It is also possible that aberrant ingression of *Sox17*$^{+/-}$ gallbladder epithelia (i.e. their detachment into the lamina propria through the broken basal lamina) partially contributes to ectopic formation of the extrahepatic duct in the cystic duct region in these mutants. Therefore, our data provide a novel mechanism for the morphogenesis and maturation of gallbladder epithelium based on the gene dosage-dependent function of *Sox17* and reveal important insights into the pathogenesis of congenital biliary atresia in mammals.

Acknowledgements

The authors wish to thank Prof. Dr Patrick P. Tam (University of Sydney) for his kind critical reading on the manuscript; Prof. Dr Sean J. Morrison (University of Michigan Medical School) for provision of *Sox17*$^{GFP/+}$ mice; Dr Miyuri Kawasumi, Dr Yoshiko Kuroda, Dr Hitomi Suzuki, Ms Kasane Kishi, Mr Minoru Fukuda and Ms Sachie Matsubara for their helpful support; and Ms Itsuko Yagihashi and Ms Taeko Nagano for their secretarial assistance. Finally, the authors wish to deeply thank Mr Yutaroh Miura for his excellent pilot/pioneer experiments on the hepatic part of this study.

Funding

This work was supported mainly by financial grants from the Ministry of Education, Science, Sports and Culture of Japan [A-21248034; S-24228005 to Y.K.; C-20590178 and 24500485 to M.K.-A.]. This work was also supported by the National Institute of Child Health and Human Development [R01 HD066121 to Y.S.]. Deposited in PMC for release after 12 months.

Competing interests statement

The authors declare no competing financial interests.

Supplementary material

Supplementary material available online at
http://dev.biologists.org/lookup/suppl/doi:10.1242/dev.086702/-/DC1

References

Artus, J., Piliszek, A. and Hadjantonakis, A. K. (2011). The primitive endoderm lineage of the mouse blastocyst: sequential transcription factor activation and regulation of differentiation by Sox17. *Dev. Biol.* **350**, 393-404.

Bamford, R. N., Roessler, E., Burdine, R. D., Saplako lu, U., dela Cruz, J., Splitt, M., Goodship, J. A., Towbin, J., Bowers, P., Ferrero, G. B. et al. (2000). Loss-of-function mutations in the EGF-CFC gene CFC1 are associated with human left-right laterality defects. *Nat. Genet.* **26**, 365-369.

Bernstein, H., Payne, C. M., Bernstein, C., Schneider, J., Beard, S. E. and Crowley, C. L. (1999). Activation of the promoters of genes associated with DNA

damage, oxidative stress, ER stress and protein malfolding by the bile salt, deoxycholate. *Toxicol. Lett.* **108**, 37-46.
Bochkis, I. M., Rubins, N. E., White, P., Furth, E. E., Friedman, J. R. and Kaestner, K. H. (2008). Hepatocyte-specific ablation of Foxa2 alters bile acid homeostasis and results in endoplasmic reticulum stress. *Nat. Med.* **14**, 828-836.
Cardinale, V., Wang, Y., Carpino, G., Cui, C. B., Gatto, M., Rossi, M., Berloco, P. B., Cantafora, A., Wauthier, E., Furth, M. E. et al. (2011). Multipotent stem/progenitor cells in human biliary tree give rise to hepatocytes, cholangiocytes, and pancreatic islets. *Hepatology* **54**, 2159-2172.
Carpentier, R., Suñer, R. E., van Hul, N., Kopp, J. L., Beaudry, J. B., Cordi, S., Antoniou, A., Raynaud, P., Lepreux, S., Jacquemin, P. et al. (2011). Embryonic ductal plate cells give rise to cholangiocytes, periportal hepatocytes, and adult liver progenitor cells. *Gastroenterology* **141**, 1432-1438, e1-e4.
Carpino, G., Cardinale, V., Onori, P., Franchitto, A., Berloco, P. B., Rossi, M., Wang, Y., Semeraro, R., Anceschi, M., Brunelli, R. et al. (2012). Biliary tree stem/progenitor cells in glands of extrahepatic and intraheptic bile ducts: an anatomical in situ study yielding evidence of maturational lineages. *J. Anat.* **220**, 186-199.
Cermenati, S., Moleri, S., Cimbro, S., Corti, P., Del Giacco, L., Amodeo, R., Dejana, E., Koopman, P., Cotelli, F. and Beltrame, M. (2008). Sox18 and Sox7 play redundant roles in vascular development. *Blood* **111**, 2657-2666.
Chu, A. S., Russo, P. A. and Wells, R. G. (2012). Cholangiocyte cilia are abnormal in syndromic and non-syndromic biliary atresia. *Mod. Pathol.* **25**, 751-757.
Clotman, F., Lannoy, V. J., Reber, M., Cereghini, S., Cassiman, D., Jacquemin, P., Roskams, T., Rousseau, G. G. and Lemaigre, F. P. (2002). The onecut transcription factor HNF6 is required for normal development of the biliary tract. *Development* **129**, 1819-1828.
Desmet, V. J. (1992). Congenital diseases of intrahepatic bile ducts: variations on the theme "ductal plate malformation". *Hepatology* **16**, 1069-1083.
Doetschman, T. (1999). Interpretation of phenotype in genetically engineered mice. *Lab. Anim. Sci.* **49**, 137-143.
Flynn, D. M., Nijjar, S., Hubscher, S. G., de Goyet, J. V., Kelly, D. A., Strain, A. J. and Crosby, H. A. (2004). The role of Notch receptor expression in bile duct development and disease. *J. Pathol.* **204**, 55-64.
Francois, M., Koopman, P. and Beltrame, M. (2010). SoxF genes: key players in the development of the cardio-vascular system. *Int. J. Biochem. Cell Biol.* **42**, 445-448.
Hara, K., Kanai-Azuma, M., Uemura, M., Shitara, H., Taya, C., Yonekawa, H., Kawakami, H., Tsunekawa, N., Kurohmaru, M. and Kanai, Y. (2009). Evidence for crucial role of hindgut expansion in directing proper migration of primordial germ cells in mouse early embryogenesis. *Dev. Biol.* **330**, 427-439.
Hartley, J. L., O'Callaghan, C., Rossetti, S., Consugar, M., Ward, C. J., Kelly, D. A. and Harris, P. C. (2011). Investigation of primary cilia in the pathogenesis of biliary atresia. *J. Pediatr. Gastroenterol. Nutr.* **52**, 485-488.
He, S., Kim, I., Lim, M. S. and Morrison, S. J. (2011). Sox17 expression confers self-renewal potential and fetal stem cell characteristics upon adult hematopoietic progenitors. *Genes Dev.* **25**, 1613-1627.
Hosking, B., François, M., Wilhelm, D., Orsenigo, F., Caprini, A., Svingen, T., Tutt, D., Davidson, T., Browne, C., Dejana, E. et al. (2009). Sox7 and Sox17 are strain-specific modifiers of the lymphangiogenic defects caused by Sox18 dysfunction in mice. *Development* **136**, 2385-2391.
Hunter, M. P., Wilson, C. M., Jiang, X., Cong, R., Vasavada, H., Kaestner, K. H. and Bogue, C. W. (2007). The homeobox gene Hhex is essential for proper hepatoblast differentiation and bile duct morphogenesis. *Dev. Biol.* **308**, 355-367.
Kalinichenko, V. V., Zhou, Y., Bhattacharyya, D., Kim, W., Shin, B., Bambal, K. and Costa, R. H. (2002). Haploinsufficiency of the mouse Forkhead Box f1 gene causes defects in gall bladder development. *J. Biol. Chem.* **277**, 12369-12374.
Kanai, Y., Kanai-Azuma, M., Noce, T., Saido, T. C., Shiroishi, T., Hayashi, Y. and Yazaki, K. (1996). Identification of two Sox17 messenger RNA isoforms, with and without the high mobility group box region, and their differential expression in mouse spermatogenesis. *J. Cell Biol.* **133**, 667-681.
Kanai-Azuma, M., Kanai, Y., Gad, J. M., Tajima, Y., Taya, C., Kurohmaru, M., Sanai, Y., Yonekawa, H., Yazaki, K., Tam, P. P. et al. (2002). Depletion of definitive gut endoderm in Sox17-null mutant mice. *Development* **129**, 2367-2379.
Kidokoro, T., Matoba, S., Hiramatsu, R., Fujisawa, M., Kanai-Azuma, M., Taya, C., Kurohmaru, M., Kawakami, H., Hayashi, Y., Kanai, Y. et al. (2005). Influence on spatiotemporal patterns of a male-specific Sox9 activation by ectopic Sry expression during early phases of testis differentiation in mice. *Dev. Biol.* **278**, 511-525.
Kim, I., Saunders, T. L. and Morrison, S. J. (2007). Sox17 dependence distinguishes the transcriptional regulation of fetal from adult hematopoietic stem cells. *Cell* **130**, 470-483.
Kohsaka, T., Yuan, Z. R., Guo, S. X., Tagawa, M., Nakamura, A., Nakano, M., Kawasasaki, H., Inomata, Y., Tanaka, K. and Miyauchi, J. (2002). The significance of human jagged 1 mutations detected in severe cases of extrahepatic biliary atresia. *Hepatology* **36**, 904-912.
Lemaigre, F. P. (2003). Development of the biliary tract. *Mech. Dev.* **120**, 81-87.
Loebel, D. A., Studdert, J. B., Power, M., Radziewic, T., Jones, V., Coultas, L., Jackson, Y., Rao, R. S., Steiner, K., Fossat, N. et al. (2011). Rhou maintains the epithelial architecture and facilitates differentiation of the foregut endoderm. *Development* **138**, 4511-4522.
Matsui, T., Kanai-Azuma, M., Hara, K., Matoba, S., Hiramatsu, R., Kawakami, H., Kurohmaru, M., Koopman, P. and Kanai, Y. (2006). Redundant roles of Sox17 and Sox18 in postnatal angiogenesis in mice. *J. Cell Sci.* **119**, 3513-3526.
Mieli-Vergani, G. and Vergani, D. (2009). Biliary atresia. *Semin. Immunopathol.* **31**, 371-381.
Nakanura, Y., Harada, K., Sato, Y. and Ikeda, H. (2010). Recent progress in the etiopathogenesis of pediatric biliary disease, particularly Caroli's disease with congenital hepatic fibrosis and biliary atresia. *Histol. Histopathol.* **25**, 223-235.
Niimi, T., Hayashi, Y., Futaki, S. and Sekiguchi, K. (2004). SOX7 and SOX17 regulate the parietal endoderm-specific enhancer activity of mouse laminin alpha1 gene. *J. Biol. Chem.* **279**, 38055-38061.
Okada, K., Kamiya, A., Ito, K., Yanagida, A., Ito, H., Kondou, H., Nishina, H. and Nakauchi, H. (2012). Prospective isolation and characterization of bipotent progenitor cells in early mouse liver development. *Stem Cells Dev.* **21**, 1124-1133.
Onitsuka, I., Tanaka, M. and Miyajima, A. (2010). Characterization and functional analyses of hepatic mesothelial cells in mouse liver development. *Gastroenterology* **138**, 1525-1535, e1-e6.
Pfister, S., Jones, V. J., Power, M., Truisi, G. L., Khoo, P. L., Steiner, K. A., Kanai-Azuma, M., Kanai, Y., Tam, P. P. and Loebel, D. A. (2011). Sox17-dependent gene expression and early heart and gut development in Sox17-deficient mouse embryos. *Int. J. Dev. Biol.* **55**, 45-58.
Sakamoto, Y., Hara, K., Kanai-Azuma, M., Matsui, T., Miura, Y., Tsunekawa, N., Kurohmaru, M., Saijoh, Y., Koopman, P. and Kanai, Y. (2007). Redundant roles of Sox17 and Sox18 in early cardiovascular development of mouse embryos. *Biochem. Biophys. Res. Commun.* **360**, 539-544.
Saund, R. S., Kanai-Azuma, M., Kanai, Y., Kim, I., Lucero, M. T. and Saijoh, Y. (2012). Gut endoderm is involved in the transfer of left-right asymmetry from the node to the lateral plate mesoderm in the mouse embryo. *Development* **139**, 2426-2435.
Schweizer, P. (1986). Treatment of extrahepatic bile duct atresia: results and long-term prognosis after hepatic portoenterostomy. *Pediatr. Surg. Int.* **1**, 30-36.
Serrano, A. G., Gandillet, A., Pearson, S., Lacaud, G. and Kouskoff, V. (2010). Contrasting effects of Sox17- and Sox18-sustained expression at the onset of blood specification. *Blood* **115**, 3895-3898.
Shimoda, M., Kanai-Azuma, M., Hara, K., Miyazaki, S., Kanai, Y., Monden, M. and Miyazaki, J. (2007). Sox17 plays a substantial role in late-stage differentiation of the extraembryonic endoderm in vitro. *J. Cell Sci.* **120**, 3859-3869.
Shin, D., Weidinger, G., Moon, R. T. and Stainier, D. Y. (2012). Intrinsic and extrinsic modifiers of the regulative capacity of the developing liver. *Mech. Dev.* **128**, 525-535.
Shiojiri, N. and Katayama, H. (1987). Secondary joining of the bile ducts during the hepatogenesis of the mouse embryo. *Anat. Embryol. (Berl.)* **177**, 153-163.
Shirai, T., Miyagi, S., Horiuchi, D., Okuda-Katayanagi, T., Nishimoto, M., Muramatsu, M., Sakamoto, Y., Nagata, M., Hagiwara, K. and Okuda, A. (2005). Identification of an enhancer that controls up-regulation of fibronectin during differentiation of embryonic stem cells into extraembryonic endoderm. *J. Biol. Chem.* **280**, 7244-7252.
Spence, J. R., Lange, A. W., Lin, S. C., Kaestner, K. H., Lowy, A. M., Kim, I., Whitsett, J. A. and Wells, J. M. (2009). Sox17 regulates organ lineage segregation of ventral foregut progenitor cells. *Dev. Cell* **17**, 62-74.
Stainier, D. Y. (2002). A glimpse into the molecular entrails of endoderm formation. *Genes Dev.* **16**, 893-907.
Sumazaki, R., Shiojiri, N., Isoyama, S., Masu, M., Keino-Masu, K., Osawa, M., Nakauchi, H., Kageyama, R. and Matsui, A. (2004). Conversion of biliary system to pancreatic tissue in Hes1-deficient mice. *Nat. Genet.* **36**, 83-87.
Tam, P. P., Kanai-Azuma, M. and Kanai, Y. (2003). Early endoderm development in vertebrates: lineage differentiation and morphogenetic function. *Curr. Opin. Genet. Dev.* **13**, 393-400.
Uemura, M., Hara, K., Shitara, H., Ishii, R., Tsunekawa, N., Miura, Y., Kurohmaru, M., Taya, C., Yonekawa, H., Kanai-Azuma, M. et al. (2010). Expression and function of mouse Sox17 gene in the specification of gallbladder/bile-duct progenitors during early foregut morphogenesis. *Biochem. Biophys. Res. Commun.* **391**, 357-363.
Viotti, M., Niu, L., Shi, S. H. and Hadjantonakis, A. K. (2012). Role of the gut endoderm in relaying left-right patterning in mice. *PLoS Biol.* **10**, e1001276.
Yamashita, R., Takegawa, Y., Sakumoto, M., Nakahara, M., Kawazu, H., Hoshii, T., Araki, K., Yokouchi, Y. and Yamamura, K. (2009). Defective development of the gall bladder and cystic duct in Lgr4- hypomorphic mice. *Dev. Dyn.* **238**, 993-1000.
Zaret, K. S. (2008). Genetic programming of liver and pancreas progenitors: lessons for stem-cell differentiation. *Nat. Rev. Genet.* **9**, 329-340.
Zaret, K. S. and Grompe, M. (2008). Generation and regeneration of cells of the liver and pancreas. *Science* **322**, 1490-1494.
Zong, Y. and Stanger, B. Z. (2011). Molecular mechanisms of bile duct development. *Int. J. Biochem. Cell Biol.* **43**, 257-264.
Zorn, A. M. and Mason, J. (2001). Gene expression in the embryonic Xenopus liver. *Mech. Dev.* **103**, 153-157.

A

		Liver				Bile duct	
		Liver weight (mg)	ratio of (+/-)/(+/+)	Incidence ratios of embryonic hepatitis		Ectopic hd formation	
B6	+/+	65.3±1.5		0/90	(0%)	5/28	(17.9%)
(N_{7-8})	+/-	42.6±4.4	(0.66)	55/88	(62.5%)	21/22	(95.5%)
ICR	+/+	97.7±2.5		0/33	(0%)	1/35	(2.9%)
	+/-	92.5±2.2	(0.95)	2/38	(5.2%)	13/38	(34.2%)
129_{SvJ}/B6	+/+	64.8±4.2		0/15	(0%)	0/15	(0%)
(N_{1-2})	+/-	59.3±2.1	(0.92)	0/12	(0%)	2/12	(16.7%)

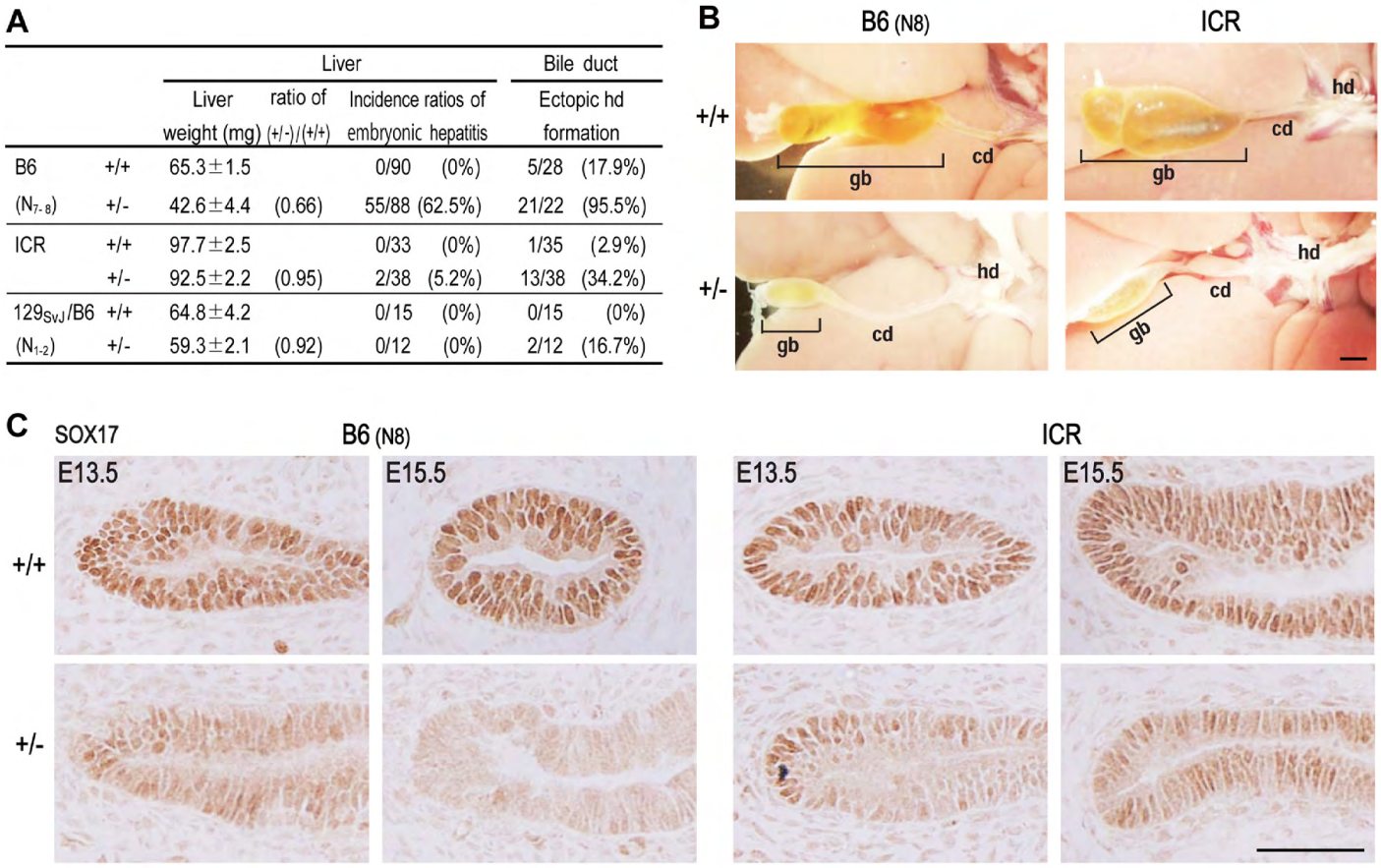

Fig. S1. Comparative phenotypes of the liver and gallbladder/bile ducts and dosage-dependent SOX17 expression in the gallbladder primordia in the *Sox17*$^{+/-}$ mice on three mixed genetic backgrounds. (**A**) Table showing comparative phenotypes [i.e. the liver weight (mg) and its ratio (*Sox17*$^{+/-}$/wild-type), and the incidence ratios of embryonic hepatitis and ectopic hepatic ducts] in the *Sox17*$^{+/-}$ embryos at 17.5 dpc on three mixed genetic backgrounds. (**B**) Gross anatomical images showing gallbladder hypoplasia at adult stage (8 weeks old) even in ICR background. The hypoplasic gallbladder in the *Sox17*$^{+/-}$ (B6) adult survivor is also shown in left lower plate. (**C**) Comparative anti-SOX17 immunostaining of the gallbladder primordia in the wild-type and *Sox17*$^{+/-}$ embryos at 13.5 and 15.5 dpc. After the gallbladder tissues were dissected from the wild-type and *Sox17*$^{+/-}$ littermates, the fixation, sectioning and staining were performed as carefully as possible under the same condition. Anti-SOX17-positive signal intensities appear to be reduced in *Sox17*$^{+/-}$ gallbladder region compared with those in wild-type counterparts in both ICR and B6 backgrounds. cd, cystic duct; hd, extrahepatic duct; gb, gallbladder. Scale bars: 1 mm in B, 50 μm in C.

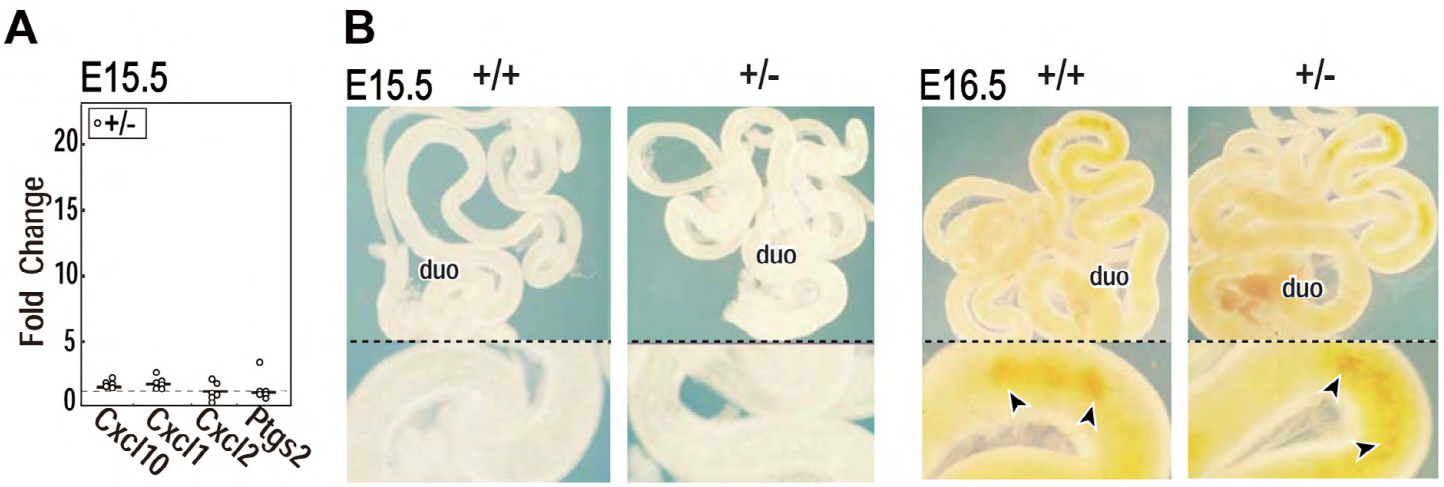

Fig. S2. No appreciable upregulation of hepatic inflammation markers in the *Sox17*$^{+/-}$ B6 livers (at 15.5 dpc) before the first biliary excretion into the fetal duodenum. (**A**) Real-time RT-PCR analysis showing normal expression levels of *Cxcl10*, *Cxcl1*, *Cxcl2* and *Ptgs2* in *Sox17*$^{+/-}$ B6 livers at 15.5 dpc. The vertical axis represents fold changes in the expression level of each liver sample relative to those of wild-type livers (the mean value was set as 1). (**B**) The gross-anatomical images of the embryonic duodenum (lower insets) and intestine before (15.5 dpc) and after (16.5 dpc) the first biliary excretion (yellow; arrowheads) into the fetal duodenum in wild-type and *Sox17*$^{+/-}$ embryos. duo, duodenum.

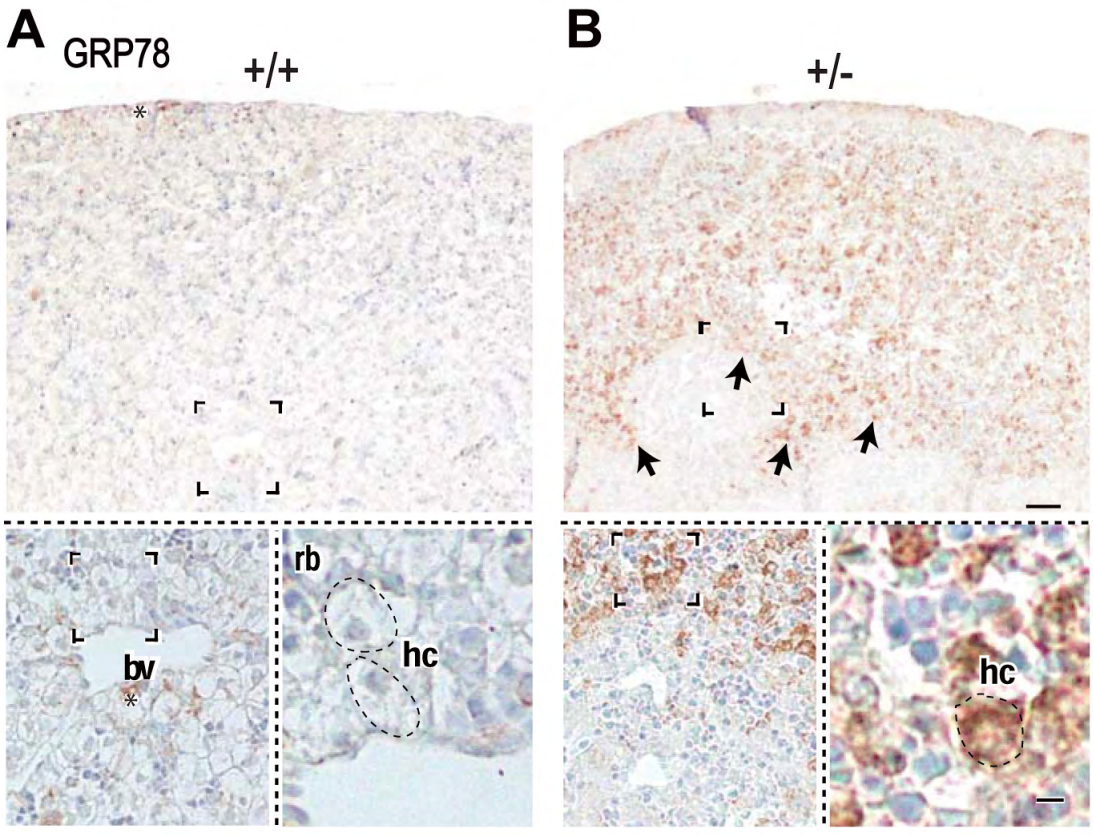

Fig. S3. Comparative anti-GRP78 immunostaining (brown) in the wild-type and *Sox17*$^{+/-}$ liver lobules. (**A**,**B**) After the liver lobules (left lateral) were dissected from the wild-type and *Sox17*$^{+/-}$ littermates at 17.5 dpc, the fixation, sectioning and staining were performed as carefully as possible under the same condition. No appreciable positive signals were detected in the wild-type liver lobules (A). GRP78-positive signals are highly detected in the hepatocytes around the degenerating peripheral region of *Sox17*$^{+/-}$ liver lobules (B, arrows). Each broken rectangle indicates the area highly magnified in the adjacent plate. asterisk, non-specific signals in the edge of the section; bv, blood vessel; hc, hepatocyte, rb, red blood (hematopoietic) cells. Scale bars: 50 μm in upper panel; 5 μm in lower-right inset.

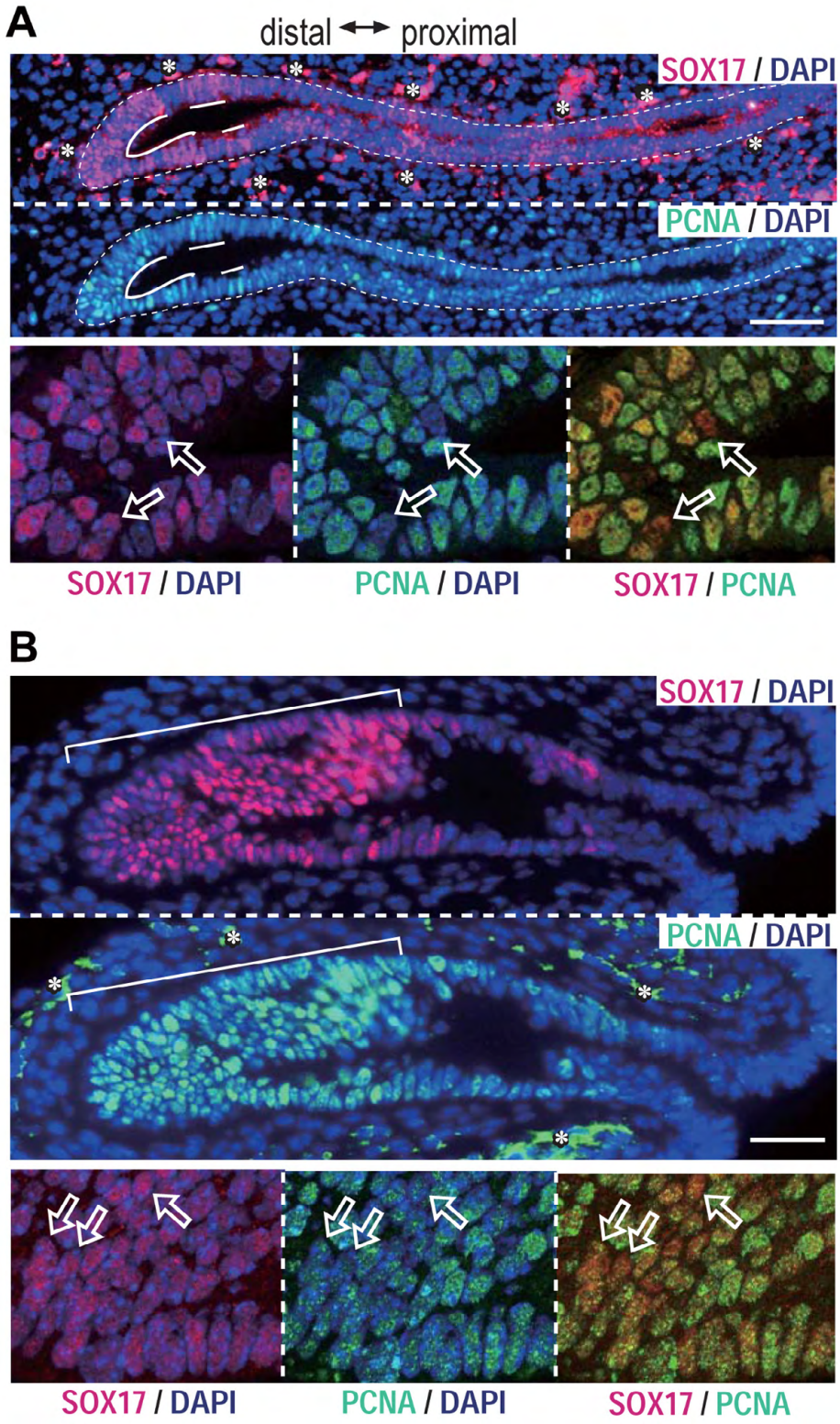

Fig. S4. Overlapping patterns of PCNA-positive and SOX17-positive domains in the bile duct epithelia of the gallbladder primordium *in vivo* and *in vitro*. (**A**,**B**) Anti-SOX17 (red fluorescence) and anti-PCNA (green fluorescence)-stained images showing the overlapping expression of SOX17/PCNA-positive domains (unbroken lines along the luminal surface in A; unbroken bars along the outer surface in B) in the gallbladder epithelial cells *in vivo* (15.5 dpc; A) and *in vitro* (a 3-day organ culture of gallbladder primordium initiated at 13.5 dpc; B). The Sox17- and PCNA-double positive cells appear to be enriched in the developing epithelial folds of the gallbladder explants. Arrows indicate SOX17-positive/PCNA-negative epithelial cells. asterisk, non-specific fluorescence in the red blood cells. Scale bar: 50 μm.

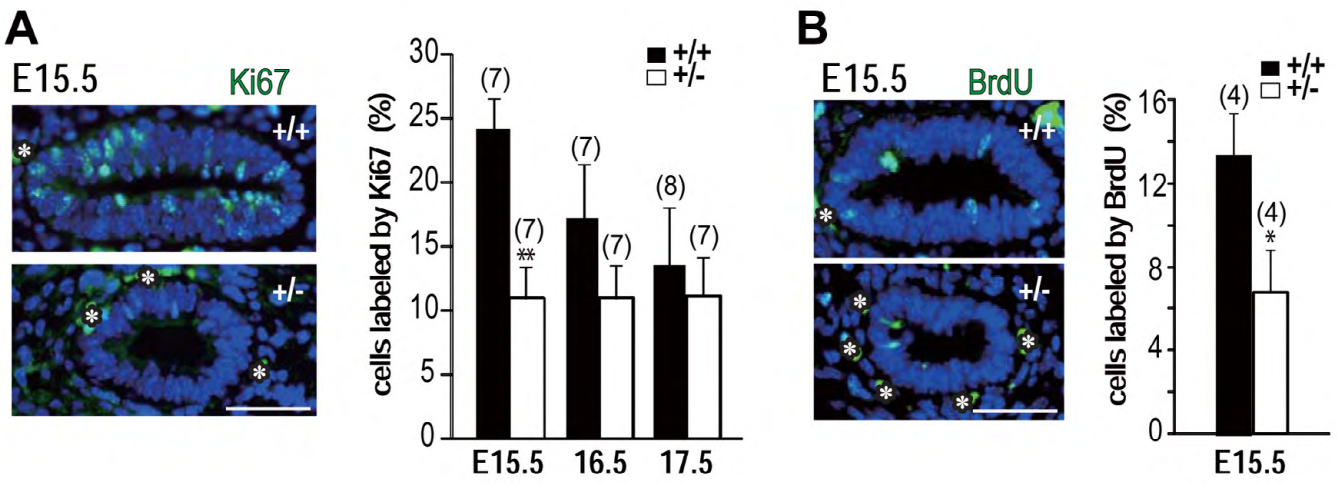

Fig. S5. Ki-67- and BrdU-labeling indices in *Sox17*$^{+/-}$ gallbladder epithelium at 15.5 to 17.5 dpc. (**A**,**B**) Anti-Ki-67 (A) and anti-BrdU (B) immunofluorescence images (left panels) and quantitative data (right graphs) showing significant reduction in both Ki-67-positive and BrdU-positive indices in *Sox17*$^{+/-}$ gallbladder epithelia at 15.5 dpc, compared with wild-type counterparts (**P<0.01 in A; *P<0.05 in B). Numbers in parentheses indicate the total number of embryos used in each group. asterisk, non-specific fluorescence in the red blood cells. Error bars represent s.e.m. Scale bar: 50 μm.

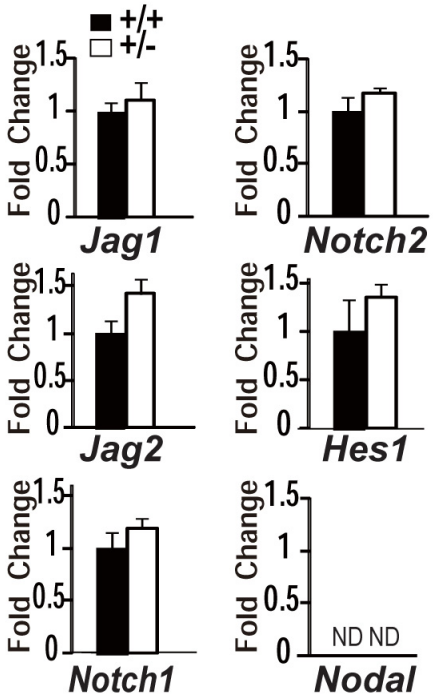

Fig. S6. No significant changes in the mRNA expression levels of notch and nodal signaling molecules in the gallbladder primordium. Real-time RT-PCR analysis showing no significant differences in mRNA expression levels of *Jag1*, *Jag2*, *Notch1*, *Notch2, Hes1* and *Nodal* between wild-type and *Sox17*$^{+/-}$ gallbladder primordia at 15.5 dpc (the mean value of wild-type gallbladder was set as 1). *Nodal* expression was undetectable in both genotypes. Error bars represent s.e.m.

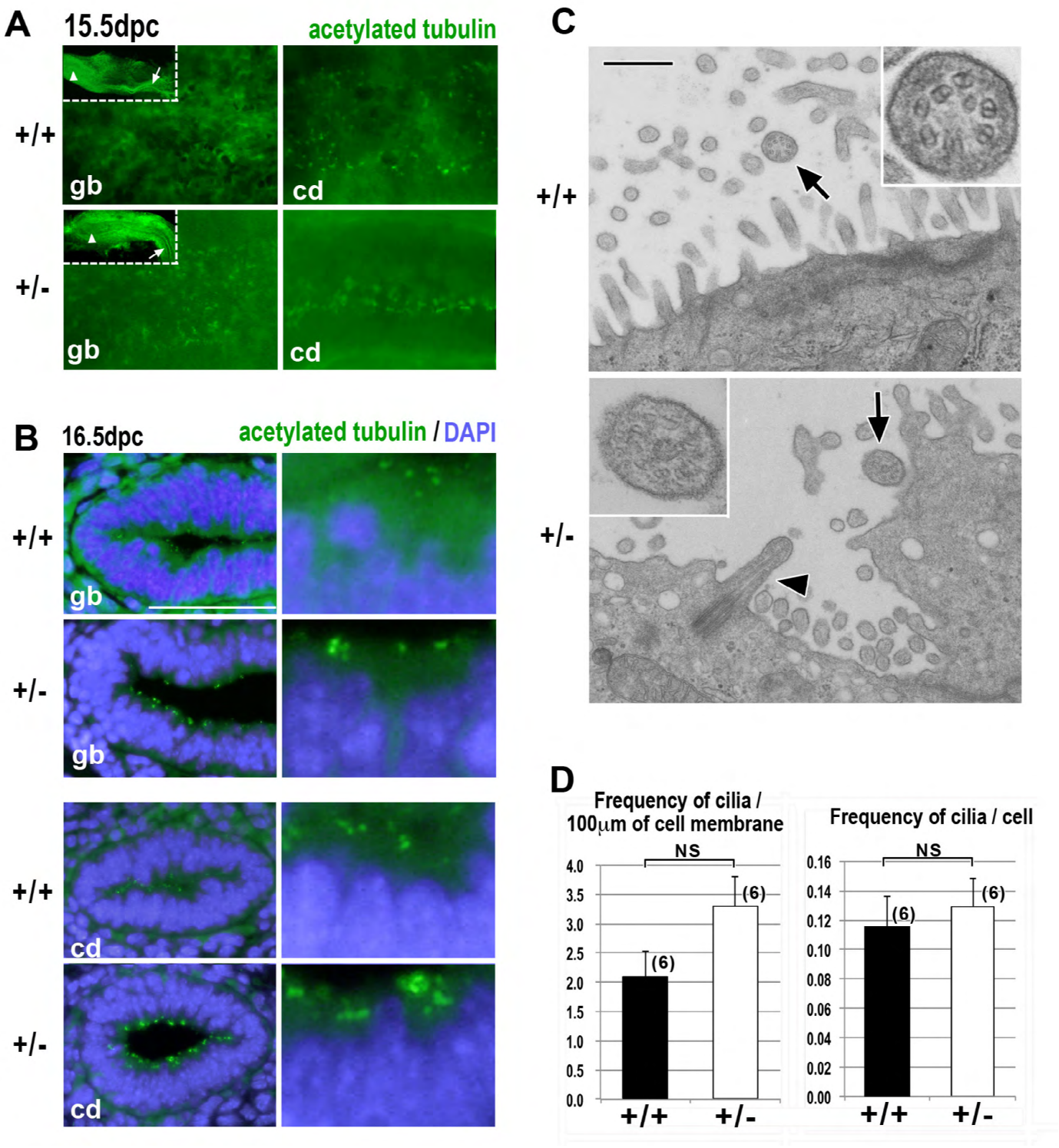

Fig. S7. No appreciable defects in distribution and frequency of primary cilia in the gallbladder and bile duct system in the *Sox17*$^{+/-}$ B6 embryos. (**A**,**B**) Whole-mount (A) and section (B) anti-acetylated tubulin staining of the gallbladder/ bile duct in wild-type and *Sox17*$^{+/-}$ B6 embryos at 15.5 and 16.5 dpc. No appreciable defects in the distribution patterns of primary cilia are found on the apical surface of the epithelial cells of *Sox17*$^{+/-}$ gallbladder (gb) and cystic duct (cd) regions. In the gallbladder region, the frequency of anti-acetylated tubulin-positive deposits appears to be increased, rather than reduced, compared with that in wild-type counterparts. In A, the insets show lower magnified images of the stained samples, in which arrowheads and arrows show the gallbladder and cystic duct regions, respectively. (**C**,**D**) Electron microscopic images (C) and quantitative data (D) showing proper formation of the primary cilia in the *Sox17*$^{+/-}$ gallbladder epithelia at 16.5 dpc. The frequency of the primary cilia per length of apical surface membrane (left graph) appears to be increased (P=0.052), rather than decreased, in the *Sox17*$^{+/-}$ gallbladder epithelia, although there were no differences in cilia frequency per cell between two genotypes (right graph). Numbers in parentheses indicate the total number of embryos used in each group. In C, the arrowhead and arrows show the sagittal and transverse (insets) images of the primary cilia, respectively. cd, cystic duct; gb, gallbladder. Error bars represent s.e.m. Scale bars: 50 μm in A,B; 0.5 μm in C.

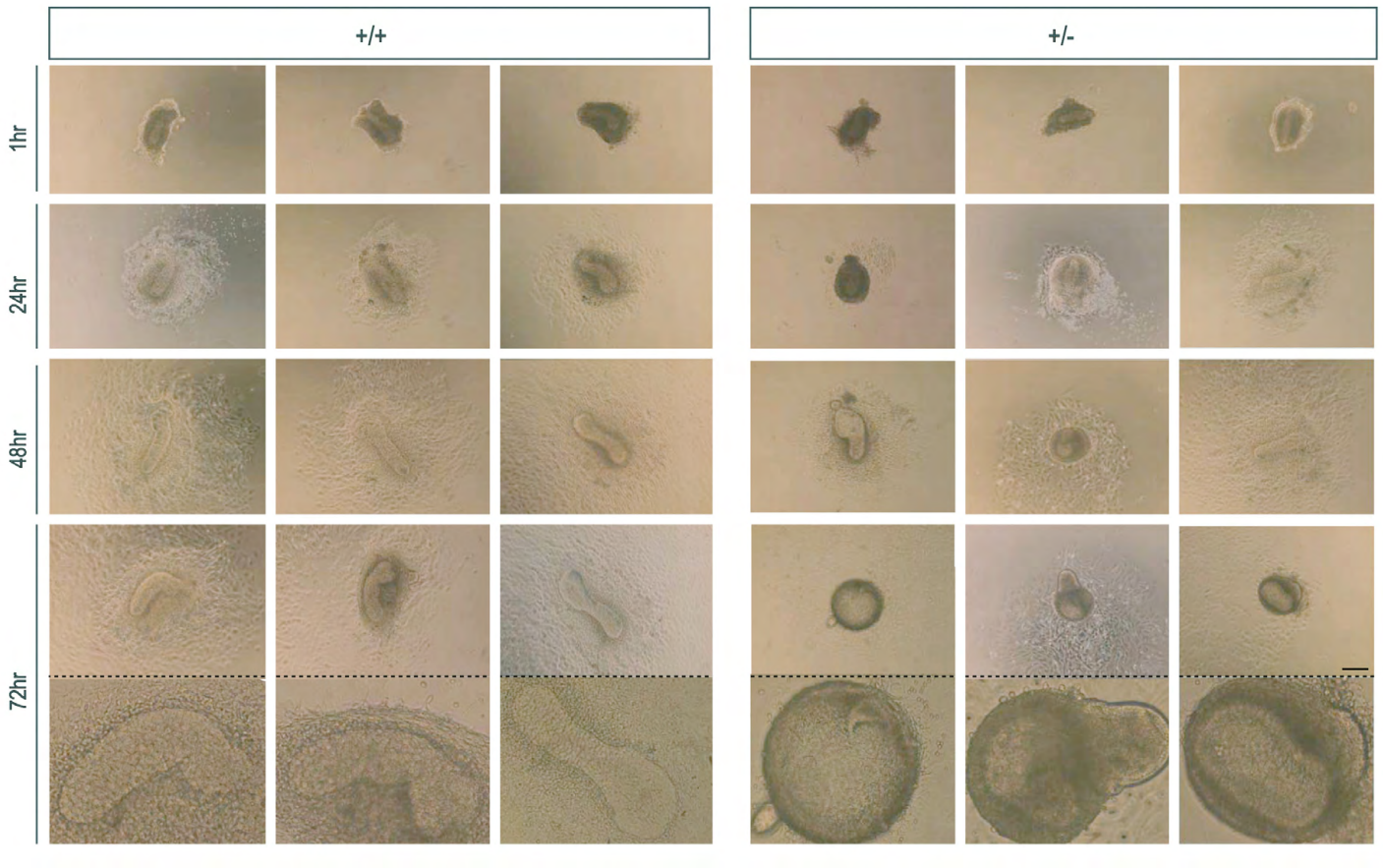

Fig. S8. Phase-contrast images of the time course of 3-day organ culture of the gallbladder primordium initiated at 13.5 dpc. Gallbladder primordia were isolated from *Sox17*$^{+/-}$ and wild-type littermates, placed on gelatin-coated plates, and then cultured in 10% fetal calf serum-DMEM at 37°C for 72 hours. In each explant, the phase-contrast images of the time course were acquired by hand with only a short culture interruption. Scale bar: 200 μm.

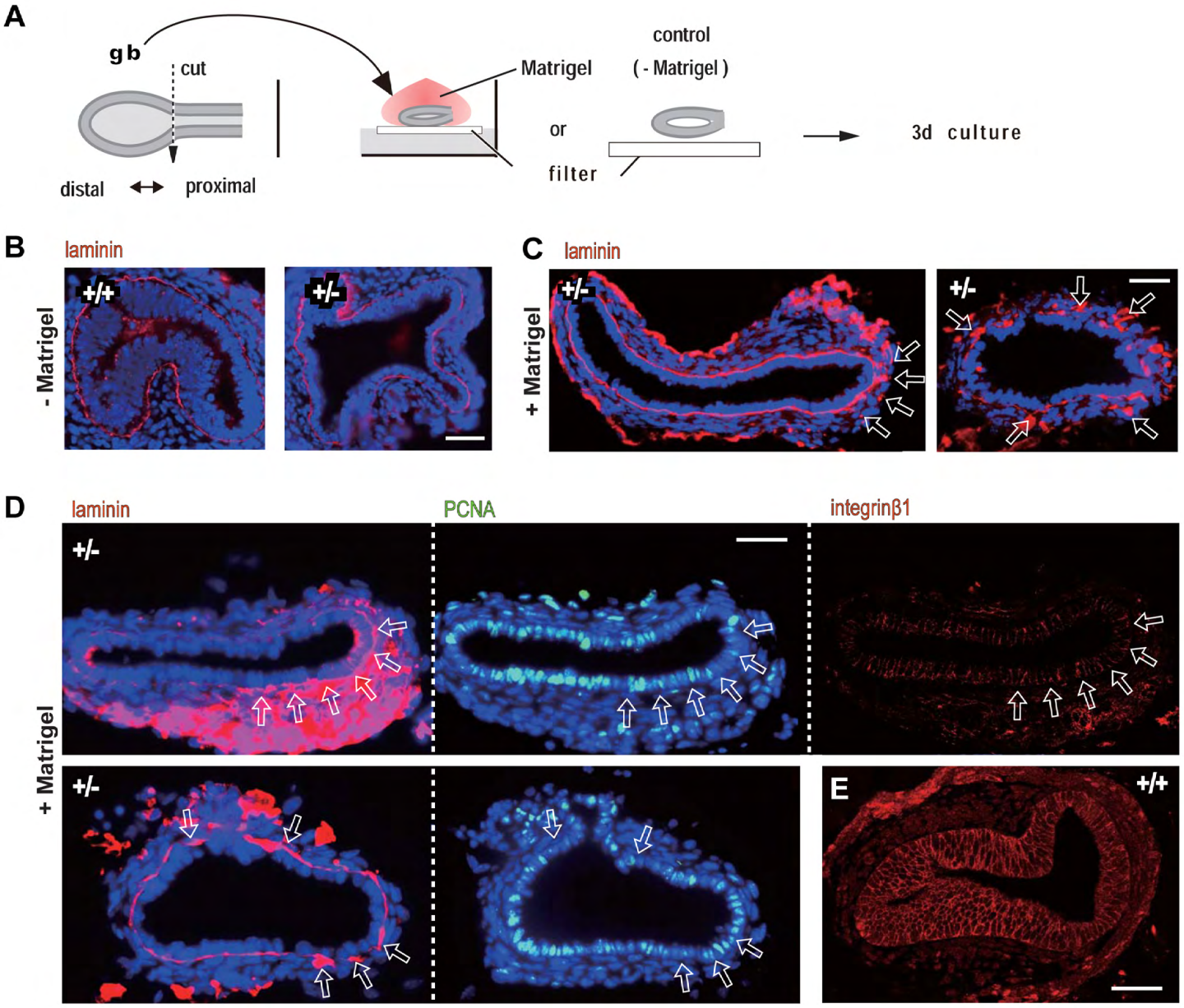

Fig. S9. Exogenous supply of basement membrane matrix (Matrigel) is not able to rescue the defects in the epithelial morphogenesis and polarized proliferation in the *Sox17*$^{+/-}$ gallbladder primordia *in vitro*. (**A**) A schematic showing the organ culture experiment of the 13.5-dpc gallbladder explants embedded in Matrigel on the filter (3 days). All gallbladder tissues were punched by a 27G needle in the presence of Matrigel before the culture initiation. (**B**) Anti-laminin staining of the control explants (in the absence of Matrigel) showing endogenous laminin distribution in the wild-type and *Sox17*$^{+/-}$ gallbladder explants. (**C**,**D**) Anti-laminin staining of the *Sox17*$^{+/-}$ gallbladder explants embedded in Matrigel, showing various distribution patterns of exogenous basement membrane matrix (C,D, arrows) around the *Sox17*$^{+/-}$ gallbladder epithelial cell layer. However, almost all of the gallbladder epithelial cells display a single cuboidal epithelial layer irrespective of whether they were directly underlined by exogenous basement membrane matrix or not. Anti-PCNA and integrin β1-stained images also show no appreciable differences in PCNA-positive domains and reduced integrin β1 expression between the epithelial cells with or without direct contact of the exogenous basement membrane matrix. (E) Anti-integrin β1 staining image of the wild-type (control) gallbladder explant. Scale bar: 50 μm.

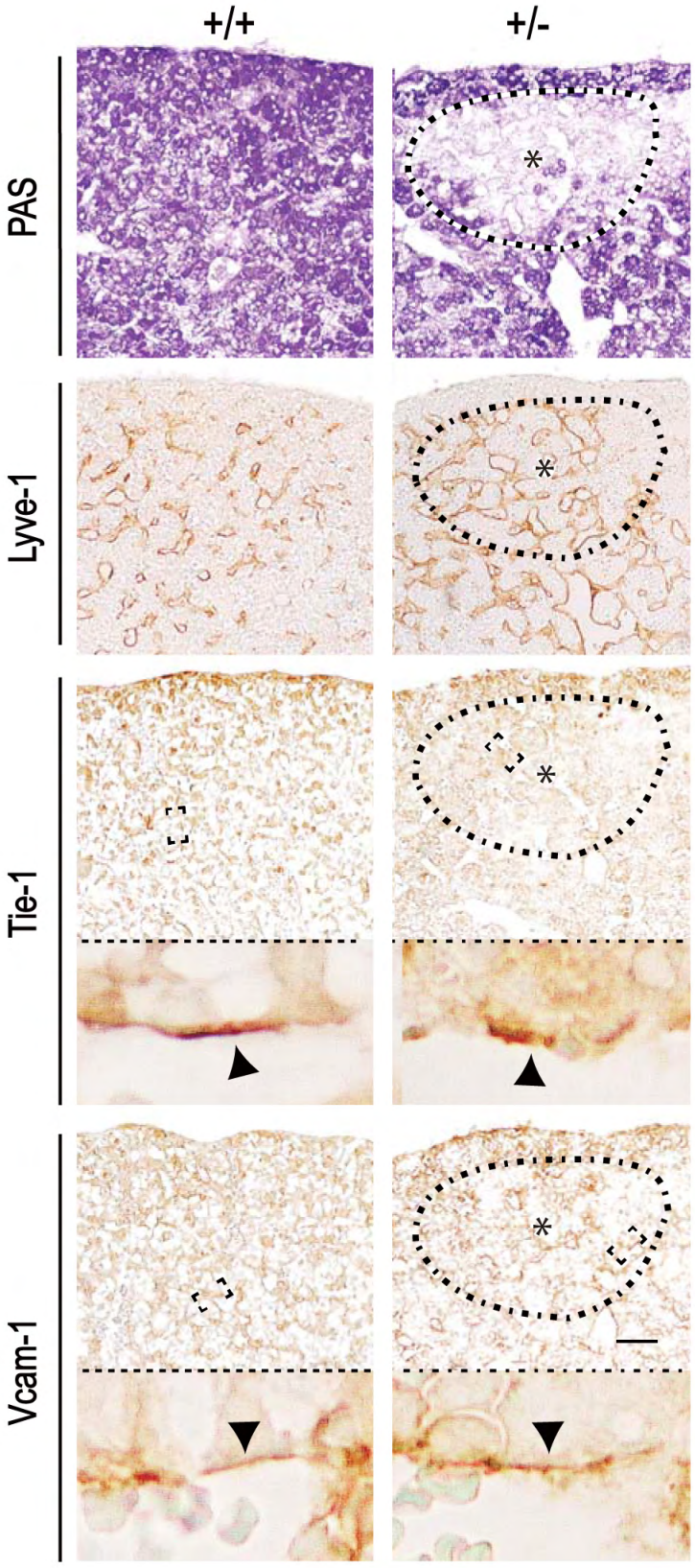

Fig. S10. No appreciable defects in the liver vasculature network of *Sox17*$^{+/-}$ livers at 17.5 dpc. Immunohistochemical analysis of continuous serial sections showing no appreciable differences in the immunoreactive expression of Lyve-1, Tie-1 and Vcam-1 in vascular endothelial cells (arrowheads) between wild-type and *Sox17*$^{+/-}$ livers (even in the degenerative region of *Sox17*$^{+/-}$ livers). The insets indicate higher-magnified images of the area surrounded by the broken rectangles in upper plates. Asterisks surrounded by dashed lines indicate degenerative regions. Scale bar: 50 μm.

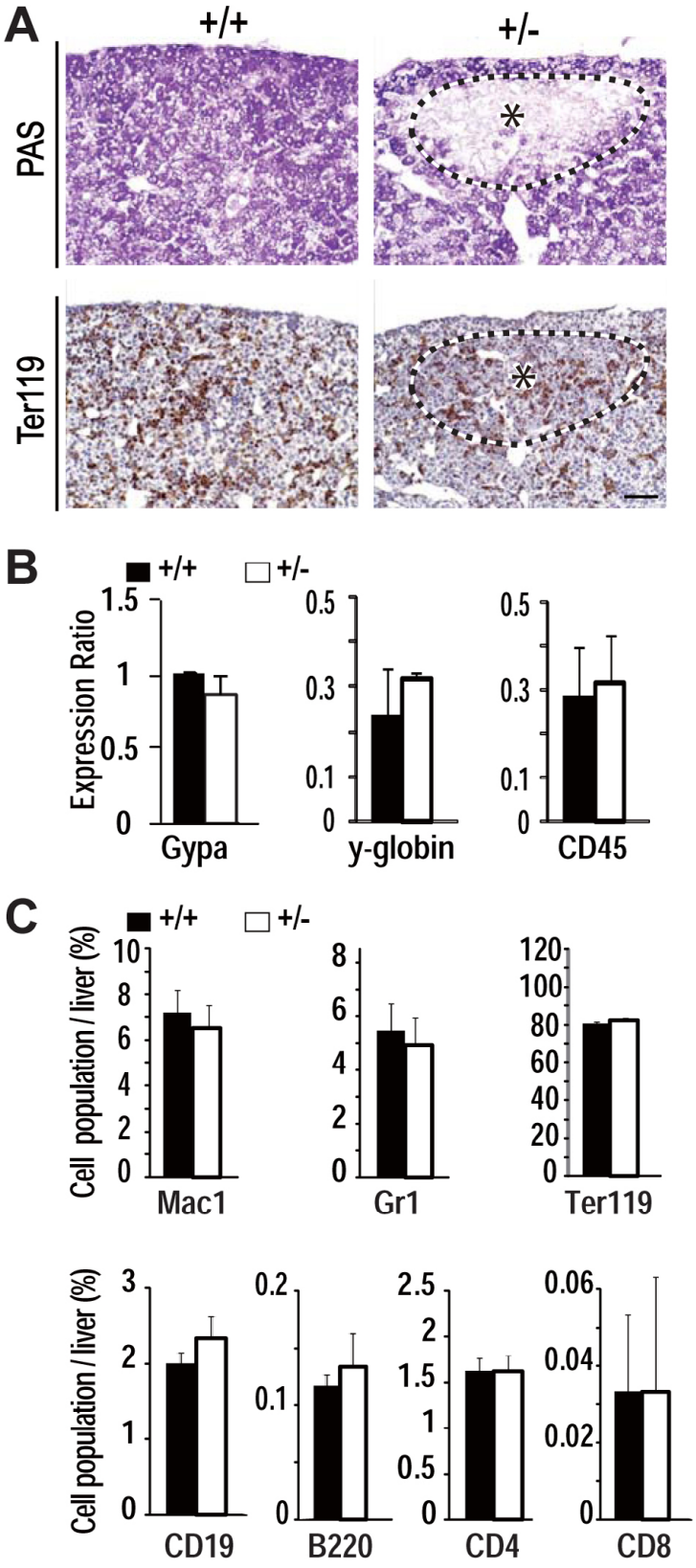

Fig. S11. No appreciable defects in hematopoietic cells of *Sox17*$^{+/-}$ livers at 17.5 dpc. (**A**) Immunohistochemical staining of serial sections showing no appreciable changes in the distribution of Ter119-positive hematopoietic cells, even in degenerative regions of *Sox17*$^{+/-}$ livers. Asterisks surrounded by dashed lines indicate degenerative regions. (**B**) Real-time RT-PCR analysis showing no significant changes in the mRNA expression levels of Gypa, Y-globin and CD45 between wild-type and *Sox17*$^{+/-}$ livers (n=4 in each). (**C**) Flow cytometric analysis using various markers specific for myeloid (Mac-1, Gr-1), erythroid (Ter119), B-lymphocytes (CD19, B220) and T-lymphocytes (CD4, CD8), showing no appreciable differences in each hematopoietic cell population between the wild-type (n=6) and *Sox17*$^{+/-}$ (n=3) livers. Scale bar: 50 μm.

Table S1. Seventeen downregulated genes in *Sox17*$^{+/-}$ livers with severe and mild phenotypes of *Sox17* heterozygote (B6) embryos compared with wild-type littermates at 17.0 dpc*

Description	Gene	Fold change‡	
		Severe	(Mild)
betaine-homocysteine methyltransferase	*Bhmt*	–5.7	(–2.8)
aldo-keto reductase family 1, member D1	*Akr1d1*	–4.9	(–3.2)
carbonic anhydrase 3	*Car3*	–4.9	(–3.0)
complement component 9	*C9*	–3.7	(–2.6)
cytochrome P450, family 7, subfamily a, polypeptide 1	*Cyp7a1*	–3.2	(–2.1)
carboxylesterase 3D	*Ces3d*	–3.2	(–3.2)
cytochrome P450, family 2, subfamily f, polypeptide 2	*Cyp2f2*	–3.2	(–3.0)
ectonucleotide pyrophosphatase/phosphodiesterase 3	*Enpp3*	–2.8	(–2.6)
cytochrome P450, family 3, subfamily a, polypeptide 11	*Cyp3a11*	–2.6	(–2.0)
alanine-glyoxylate aminotransferase 2-like 1	*Agxt2l1*	–2.5	(–2.3)
RIKEN cDNA C730007P19 gene (sulfotransferase family 2A, dehydroepiandrosterone (DHEA)-preferring, member 2)	*C730007 P19Rik* (*Sult2a2*)	–2.5	(–3.7)
SPARC related modular calcium binding 2	*Smoc2*	–2.5	(–2.0)
gelsolin	*Gsn*	–2.5	(–2.0)
predicted gene 7969	*Gm7969*	–2.3	(–3.0)
GLE1 RNA export mediator (yeast)	*Gle1*	–2.3	(–2.0)
solute carrier family 22 (organic anion transporter), member 8	*Slc22a8*	–2.0	(–2.1)
expressed sequence AI317395	*AI317395*	–2.0	(–2.0)

*Microarray expression analyses were performed using the cDNA samples collected from the central proximal region of the liver lobules in which any degenerative area was detected based on gross anatomy, even in the severe group. In the mild group, the cDNA samples were also prepared from the proximal regions of the liver lobules.

‡The fold change represents the difference in expression levels in livers between *Sox17*$^{+/-}$ and wild-type littermates. Differential expression was defined as a difference of twofold or more.